NEUROSCIENCE

A top-down insular cortex circuit crucial for non-nociceptive fear learning

Junho Han[1,2], Boin Suh[1,2], Jin-Hee Han[1,2]*

Understanding how threats drive fear memory formation is crucial to understanding how organisms adapt to environments and treat threat-related disorders such as PTSD. While traditional Pavlovian conditioning studies have provided valuable insights, the exclusive reliance on electric shock as a threat stimulus has limited our understanding of diverse threats. To address this, we developed a conditioning paradigm using a looming visual stimulus as an unconditioned stimulus (US) in mice and identified a distinct neural circuit for visual threat conditioning. Parabrachial CGRP neurons were necessary for both conditioning and memory retrieval. Upstream neurons in the posterior insular cortex (pIC) responded to looming stimuli, and their projections to the parabrachial nucleus (PBN) induced aversive states and drove conditioning. However, this pIC-to-PBN pathway was not required for foot-shock conditioning. These findings reveal how non-nociceptive visual stimuli can drive aversive states and fear memory formation, expanding our understanding of aversive US processing beyond traditional models.

INTRODUCTION

In dynamic environments, animals must learn to recognize sensory cues and contextual information associated with threats to generate appropriate defensive responses and enhance survival. While adaptive learning is essential, maladaptive fear memories are implicated in anxiety-related disorders, including post-traumatic stress disorder (PTSD). Thus, understanding how threats drive fear memory formation is crucial for developing effective treatments (*1*). To investigate the neural mechanisms of fear learning, Pavlovian fear conditioning has been widely used across various species, particularly rodents (*2*, *3*). In this paradigm, a neutral sensory cue [conditioned stimulus (CS)] is paired with an aversive stimulus [unconditioned stimulus (US)], leading to fear responses upon CS re-exposure. This model has significantly advanced our understanding of fear memory formation (*4*–*8*). However, research has predominantly relied on electric foot shocks as the primary US, limiting our understanding of fear learning driven by other types of threats.

In natural environments, threats are not exclusively nociceptive. Predator-associated cues, such as visual or chemical signals, elicit fear-related behaviors such as freezing and escape (*9*–*11*). Although non-nociceptive, these stimuli can induce aversive affective states, leading to fear learning, which is critical for survival by enabling avoidance of physical harm. Previous studies have used live predators and predator odors as non-nociceptive US in rodent fear learning models (*9*, *10*), identifying key brain regions involved in odor-induced fear learning, including the basolateral amygdala (BLA) (*12*), ventral hippocampus (vHPC) (*13*), medial amygdala (MeA) (*14*), and posterior insular cortex (pIC) (*15*). However, findings on odor-based fear conditioning are inconsistent (*16*–*19*), as different predator odors vary in effectiveness (*10*, *20*) and activate distinct brain regions (*18*). In addition, odor stimuli are difficult to control precisely, complicating circuit-level investigations.

In contrast, visual threat stimuli offer precise experimental control and cross-species applicability. Rapidly looming visual stimuli have been shown to trigger immediate defensive responses in rodents (*11*, *21*), frogs (*22*), fish (*23*, *24*), primates (*25*), and humans (*26*, *27*). A pioneering study established a visual threat model in mice using an overhead looming dark disc mimicking an approaching aerial predator (*11*). Given their advantages, visual threats seem to offer an ideal framework for developing novel non-nociceptive fear learning models.

Traditionally, US pathways in fear learning have been identified using foot-shock stimuli (*8*, *28*–*31*). Among these, the thalamus and parabrachial nucleus (PBN) in the brainstem are recognized as key ascending nociceptive pathways. The thalamus has long been considered central to nociceptive US processing due to its widespread projections across the brain (*32*–*36*). However, in addition to the thalamus, recent evidence also highlights the PBN as an essential US pathway, transmitting pain-related signals to the central nucleus of the amygdala (CeA) and other downstream regions (*37*). Han *et al.* (*37*) demonstrated that calcitonin gene-related peptide (CGRP)–expressing neurons in the PBN ($CGRP^{PBN}$ neurons) are essential for foot-shock conditioning in mice and that optogenetic activation of $CGRP^{PBN}$-CeA pathway induces fear learning.

$CGRP^{PBN}$ neurons respond not only to electric shocks but also to various non-nociceptive stimuli (*38*, *39*), including visual threats, suggesting a potential role in non-nociceptive fear learning. However, whether $CGRP^{PBN}$ neurons process US signals during non-nociceptive fear learning remains unclear. Furthermore, unlike nociceptive pathways, which are known to originate from the spinal cord and periaqueductal gray (PAG) (*40*–*42*), the upstream sources conveying non-nociceptive input to PBN neurons remain unidentified.

Here, we developed a threat conditioning paradigm in mice using the previously established looming visual threat. Through this model, we identified PBN^{CGRP} neurons and a distinct pIC-to-PBN top-down circuit as essential for visual threat conditioning. Notably, this circuit was not required for foot-shock conditioning. Furthermore, the pIC-to-PBN circuit was sufficient to induce aversive affective states and drive threat conditioning as a US. These findings highlight its role in processing threat-relevant, non-nociceptive visual information, independent of sensory pain pathways.

[1]Department of Biological Sciences, Korea Advanced Institute of Science and Technology, Daejeon 34141, South Korea. [2]KAIST Institute for the BioCentury, Korea Advanced Institute of Science and Technology, Daejeon 34141, South Korea.
*Corresponding author. Email: han.jinhee@kaist.ac.kr

RESULTS

Looming visual stimuli drive threat conditioning as a US

We aimed to develop a visual threat conditioning model using a looming visual stimulus as a US. The stimulus consisted of a rapidly expanding dark disc (5° to 35° visual angle in 300 ms), which remained at full size for 500 ms. First, we confirmed that this stimulus induces innate defensive responses in mice. Exposure to 10 consecutive looming stimuli elicited robust freezing, either immediately or following an escape response (Fig. 1, A to C). Eight animals exhibited immediate freezing, while the remaining two initially escaped before freezing. A previous study (*43*) reported predominant escape-freezing responses over immediate freezing in a no-shelter condition. However, differences in experimental conditions, particularly looming stimulus parameters, may account for these discrepancies. Notably, another study (*44*) used looming stimuli similar to ours and reported that mice primarily exhibited immediate freezing in a no-shelter condition, consistent with our findings.

Given that looming stimuli pose no actual harm, we tested for habituation. Mice exposed to looming stimuli across 5 days showed no substantial reduction in freezing (fig. S1, A and B). However, when the same stimulus was repeatedly presented within short intervals [five stimuli per session, repeated 10 times with 120-s intertrial intervals (ITIs)], freezing responses declined after the seventh exposure, indicating habituation (fig. S1, D and E). This reduction in freezing was not due to a shift in defensive behavioral patterns, as repeated looming exposures did not increase escape behavior probability (fig. S1, C and F). While notable habituation was observed after the seventh trial, some mice exhibited a decrease in freezing levels to looming stimuli relative to baseline freezing starting from the sixth trial (fig. S1G). Based on these findings, we used five CS-US pairings in subsequent conditioning experiments.

To determine whether looming stimuli can serve as an effective US, we paired a neutral auditory tone (2.7 kHz, 80 dB) as a CS with five consecutive looming stimuli as a US (looming US). In the paired group, the tone was presented for 20 s, overlapping with the final 4 s

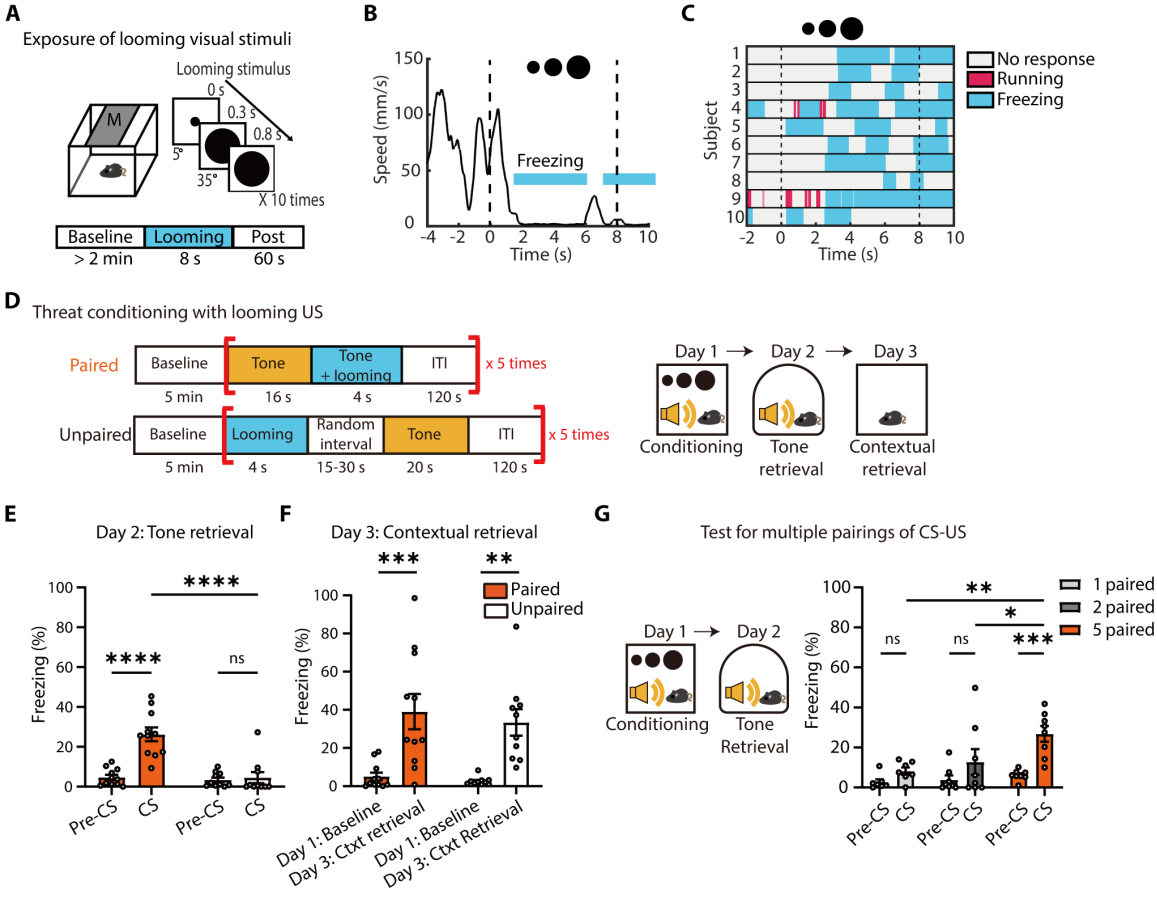

Fig. 1. Looming visual stimuli drive formation of auditory and contextual fear memory in mice. (**A**) Schematic of behavioral tests for exposure of looming visual stimuli (a 10 times repeat of a single looming for 8 s). (**B**) Changes in movement speed of mice in response to looming visual stimuli. The blue shaded bars indicate a period during which mice displayed freezing behavior. (**C**) Ethogram showing defensive behavioral responses to the presentation of looming visual stimuli. Mice displayed robust freezing, either immediately or following an escape response ($N = 10$, 8 mice showed immediate freezing and other 2 mice showed escape-freezing). (**D**) Schematic of a threat conditioning protocol with looming visual stimuli. (**E**) Auditory fear memory was formed only in the paired group (paired group, $N = 11$; Unpaired group, $N = 10$; Repeated measures (RM) two-way ANOVA, time × group, $F_{1,19} = 17.2$, $P = 0.0005$). (**F**) Both paired and unpaired groups show elevated levels of contextual freezing during re-exposure to the conditioning chamber on day3 (RM two-way ANOVA, time, $F_{1,19} = 36.38$, $P < 0.0001$). (**G**) Single and double pairings of tone CS and looming US were not effective in driving the formation of auditory fear memory (single-paired group, $N = 7$; double-paired group, $N = 8$; five-times paired group, $N = 8$; RM two-way ANOVA, group, $F_{2,20} = 4.500$, $P = 0.0243$; right). All data are means ± SEM. *$P < 0.05$, **$P < 0.01$, ***$P < 0.001$, and ****$P < 0.0001$. ns, not significant.

of the looming US. In the unpaired group, the US and CS were presented separately with a randomized 15- to 30-s interval (Fig. 1D). During the retrieval test in a different context, only the paired group exhibited robust freezing to the tone (Fig. 1E). Contextual fear memory was also assessed by re-exposing mice to the original conditioning chamber, where both groups showed elevated freezing levels (Fig. 1F). Additional experiments revealed that fewer than five CS-US pairings failed to establish robust conditioning (Fig. 1G). These results demonstrate that a non-nociceptive visual threat can drive robust fear learning as a US in mice.

CGRP^{PBN} neurons selectively respond to looming US and acquired tone CS, but not to neutral stimuli.

The PBN is a major ascending nociceptive pathway with extensive connections to the CeA and hypothalamus (*45*, *46*), regulating emotional behaviors and autonomic responses. This suggests its primary role in the affective pain processing rather than sensory pain perception. Affective pain, defined as the emotional unpleasantness of pain (*47*–*50*), drives avoidance behavior, facilitating fear learning. Supporting this, CGRP^{PBN} neurons are essential for foot-shock conditioning, and optogenetic activation of the CGRP^{PBN}-CeA pathway induces fear memory formation (*37*). Beyond nociceptive processing, CGRP^{PBN} neurons also respond to various non-nociceptive aversive stimuli (*39*) and regulate food neophobia (*38*), suggesting a broader function in aversive state encoding. These findings indicate that the PBN serves as a general danger-detection hub (*51*), integrating diverse aversive signals and regulating emotional behaviors. Thus, we reasoned that CGRP^{PBN} neurons may also contribute to fear memory formation in response to visual threats.

First, to verify whether CGRP^{PBN} neurons specifically respond to looming visual stimuli, we performed in vivo fiber photometry calcium recordings in CGRP^{PBN} neurons during exposure to looming and flickering stimuli (a nonthreatening control; Fig. 2A). Cre-dependent adeno-associated virus (AAV) encoding GCaMP6m was injected into the PBN of *Calca*^{Cre} transgenic mice (*52*), in which Cre recombinase is specifically expressed in CGRP^{+} neurons, with an optic fiber implanted above the injection site (Fig. 2B). While flickering stimuli failed to induce freezing, looming threats elicited strong freezing responses (Fig. 2C). Correspondingly, CGRP^{PBN} neurons exhibited no calcium activation in response to flickering stimuli but showed pronounced and sustained activation (~1 min) following looming threats (Fig. 2, D to G). These results demonstrate that CGRP^{PBN} neurons selectively respond to threatening visual stimuli rather than neutral visual cues.

Next, we examined CGRP^{PBN} activity during visual threat conditioning and tone retrieval tests. Mice were divided into paired and unpaired conditioning groups (Fig. 2H). As expected, both groups showed increased CGRP^{PBN} activity in response to the looming US during conditioning (Fig. 2, I to L). However, during retrieval, only the paired group exhibited increased calcium activity in response to the tone CS (Fig. 2, M to O). These findings suggest that following conditioning, CGRP^{PBN} neurons encode the acquired danger value of the tone CS, likely through synaptic plasticity-dependent mechanisms.

CGRP^{PBN} neurons are required for fear memory formation and its retrieval, but not for innate defensive response to a visual threat

To assess the necessity of CGRP^{PBN} neurons in visual threat conditioning, we inactivated them using tetanus toxin light chain (TetTox) (*53*). Cre-dependent AAV encoding TetTox and dTomato was injected into the PBN of *Calca*^{Cre} mice, with tdTomato alone serving as a control (Fig. 3A). Post hoc histological analysis confirmed restricted viral expression in the PBN (Fig. 3B). Open-field tests confirmed no locomotor or anxiety differences between groups before conditioning (Fig. 3C).

During conditioning, both TetTox and control groups exhibited similar freezing to the looming US (first CS-US pairing), indicating that CGRP^{PBN} neurons are not essential for innate defensive responses to visual threats (Fig. 3D), consistent with prior studies (*39*). This finding was further validated in an independent experiment (fig. S2, A and B). However, fear memory formation was markedly impaired—TetTox-expressing mice showed no appreciable increase in freezing to the conditioned tone or context, whereas control mice exhibited robust freezing (Fig. 3, E and F). This suggests that CGRP^{PBN} neurons are required for fear learning but not for reflexive defensive behaviors to looming stimuli.

To further investigate the role of CGRP^{PBN} neurons in visual threat conditioning and memory retrieval, we performed optogenetic inhibition. Cre-dependent AAV encoding eNpHR3.0-EYFP or EYFP alone was injected into the PBN of *Calca*^{Cre} mice, with an optic fiber implanted above the injection site. Light delivery inactivated CGRP^{PBN} neurons throughout conditioning, beginning at the onset of the first US presentation and continuing until the session concluded (Fig. 3G). Histological analysis confirmed highly restricted eNpHR3.0 expression in the PBN (Fig. 3H).

Consistent with the TetTox experiment, immediate freezing responses (measured during first CS-US pairing) were unaffected (Fig. 3I). However, fear memory formation was abolished in the eNpHR3.0 group (Fig. 3J). In a separate experiment, inhibition of CGRP^{PBN} neurons during retrieval, rather than conditioning, resulted in notably impaired freezing to the tone CS, indicating a role in memory retrieval (Fig. 3, K and L). Together, these findings demonstrate that CGRP^{PBN} neurons are required for fear memory formation and retrieval but are dispensable for innate defensive responses to visual threats.

pIC and SC cells projecting to the CGRP^{PBN} neurons are activated by looming visual stimuli

CGRP^{PBN} neurons are critical for visual threat conditioning, but their upstream non-nociceptive inputs remain unclear. While nociceptive stimuli are relayed via the spinal cord or PAG (*37*, *40*–*42*), the pathway conveying non-nociceptive US information is less understood. To identify CGRP^{PBN} inputs, we performed monosynaptic retrograde tracing by injecting Cre-dependent AAV-hsyn-DIO-TVA-HA-N2cG into the PBN of *Calca*^{Cre} mice, followed by SADB19-GFP rabies virus (fig. S3A). Starter cells were localized exclusively in the PBN (fig. S3B), and retrogradely labeled neurons were observed in ipsilateral and contralateral brain regions associated with emotional processing, sensory integration, and motor functions, including the pIC, CeA, PAG, and superior colliculus (SC) (fig. S3, C to E).

To determine which of these inputs are activated by visual threats, we analyzed c-Fos expression in projection neurons following looming or flickering stimuli. Mice injected bilaterally with AAV helper and rabies virus were exposed to either looming or flickering stimuli (Fig. 4A and fig. S4A). Only looming stimuli substantially increased freezing behavior (Fig. 4B). We analyzed c-Fos expression in fear- and vision-related upstream regions, including the insular cortex (IC), CeA, PAG, and SC. Anatomically, CGRP^{PBN}-projecting neurons

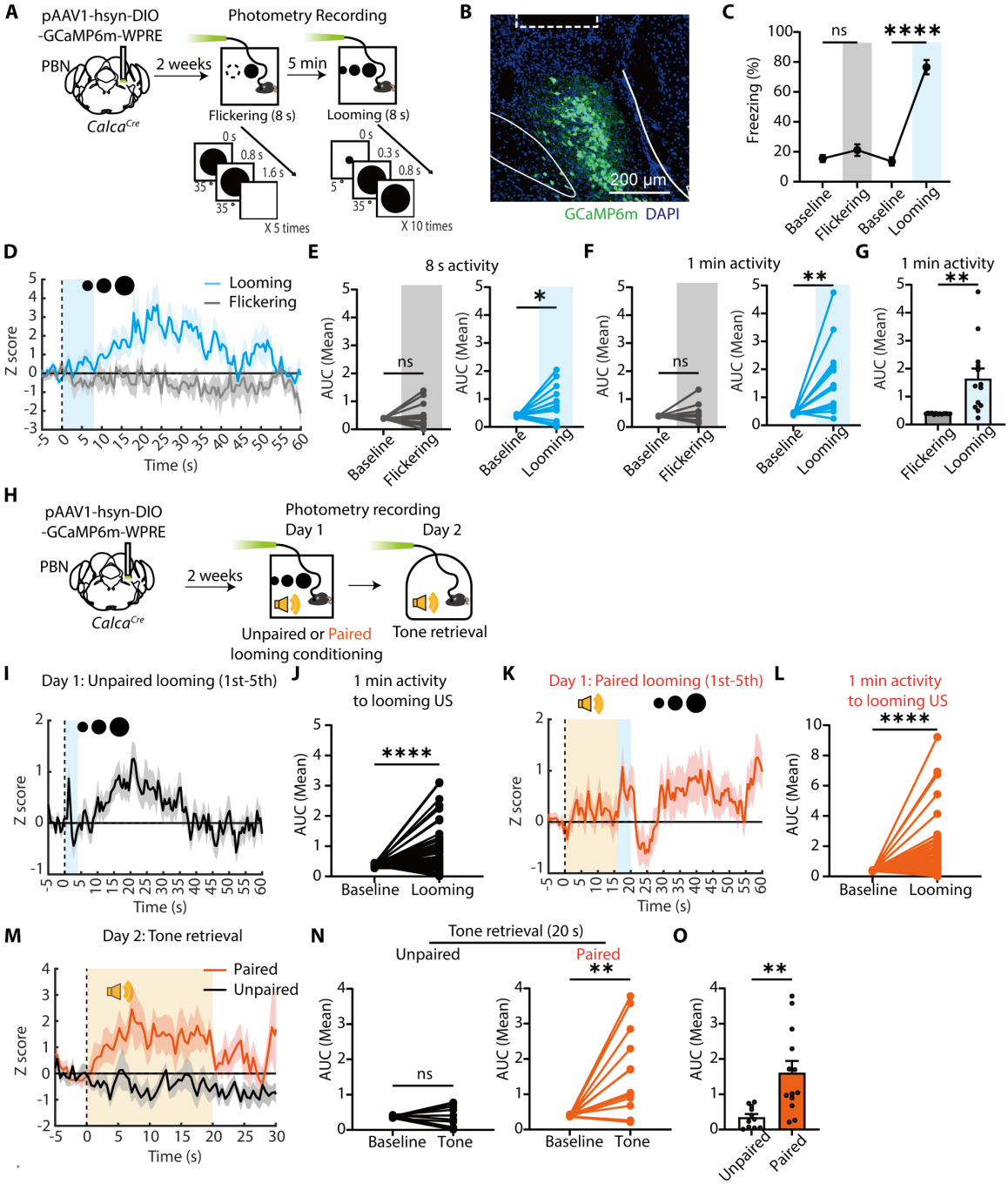

Fig. 2. CGRP^{PBN} neurons selectively respond to looming US and acquired tone CS, but not to neutral stimuli. (**A**) Schematic of fiber photometry recordings in CGRP^{PBN} neurons during visual stimuli. (**B**) Representative image of GCaMP6m expression in the PBN; the dotted rectangle marks the optic fiber location. (**C**) Freezing levels during flickering and looming stimuli ($N = 13$ mice; RM one-way ANOVA, Time, $F_{12,36} = 2.786$, $P = 0.0087$). (**D**) *z*-scored calcium activity (means ± SEM) during visual stimuli. (**E** and **F**) Average area under the curve (AUC) comparison of calcium activity during visual stimuli [(E); flickering; $N = 13$ mice; two-tailed paired *t* test, $t_{12} = 0.6077$, $P = 0.5547$; looming; $t_{12} = 2.221$, $P = 0.0464$] and during 1 min [(F); flickering; $t_{12} = 0.6251$, $P = 0.5436$; looming; $t_{12} = 3.482$, $P = 0.0045$]. (**G**) AUC comparison between flickering and looming stimuli ($t_{12} = 3.541$, $P = 0.0041$). (**H**) Schematic of fiber photometry recordings of CGRP^{PBN} neurons during visual threat conditioning. (**I** to **J**) *z*-scored calcium activity of CGRP^{PBN} neurons in the unpaired group during the first to fifth exposures to looming US [(J); $N = 55$ trials; two-tailed Wilcoxon matched-pairs signed rank test, $W = -1042$, $P < 0.0001$]. (**K** and **L**) z-scored calcium activity of CGRP^{PBN} neurons in the paired group during the first to fifth exposures to looming US [(L); $N = 65$ trials; two-tailed Wilcoxon matched-pairs signed-rank test, $W = -1261$, $P < 0.0001$]. (**M**) *z*-scored calcium activity of CGRP^{PBN} neurons during the tone retrieval test. (**N**) Average AUC of calcium activity in the unpaired (left; two-tailed paired *t* test, $t_{10} = 0.3602$, $P = 0.7262$) and paired groups (right; $t_{12} = 3.714$, $P = 0.0030$) during the tone retrieval test. (**O**) Comparison of AUC between the two groups during the tone retrieval test (two-tailed unpaired *t* test, $t_{22} = 3.431$, $P = 0.0024$). All data are means ± SEM. $^*P < 0.05$, $^{**}P < 0.01$, and $^{****}P < 0.0001$.

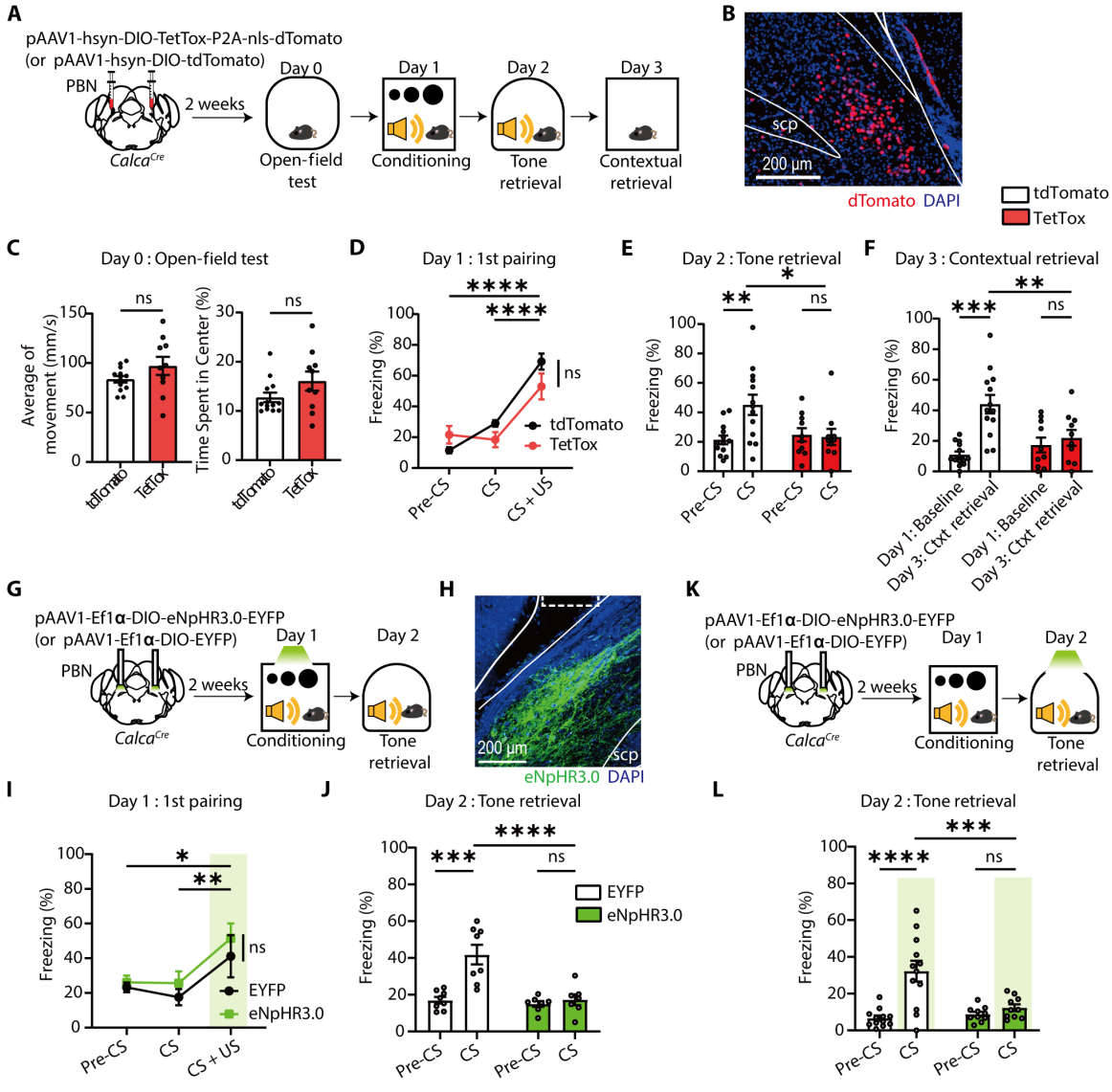

Fig. 3. The inhibition of CGRP^{PBN} neurons impairs fear memory formation and retrieval but not innate defensive behavior to looming stimuli. (**A**) Schematic of TetTox-mediated inhibition of CGRP^{PBN} neurons during visual threat conditioning. (**B**) Representative image showing the expression of dTomato in the PBN, especially in the external lateral subdivision of PBN (PBel). Scale bars, 200 μm. SCP, superior cerebellar peduncle. (**C**) Average of movement (left; TetTox, $N = 10$; tdTomato, $N = 13$; two-tailed unpaired t test, $t_{21} = 1.518$, $P = 0.1439$) and center zone time (right, two-tailed Mann-Whitney test, $U = 46$, $P = 0.2569$) were comparable between groups. (**D**) Freezing levels during the first CS-US pairing on day 1 (RM two-way ANOVA, time × group, $F_{2,42} = 5.334$, $P = 0.0086$). (**E** and **F**) TetTox inhibition of CGRP^{PBN} neurons impairs auditory [(E); RM two-way ANOVA, time × group, $F_{1,21} = 7.251$, $P = 0.0136$] and contextual fear memory [(F); RM two-way ANOVA, time × group $F_{1,21} = 7.798$, $P = 0.0109$]. (**G**) Schematic of optogenetic inhibition of CGRP^{PBN} neurons during visual threat conditioning. (**H**) Representative image of eNpHR3.0-EYFP expression in CGRP^{PBN} neurons; the dotted rectangle marks the optic fiber tip location. Scale bar, 200 μm. (**I**) Freezing during the first CS-US pairing (eNpHR3.0, $N = 7$; EYFP, $N = 8$; RM two-way ANOVA, time, $F_{2,26} = 7.167$, $P = 0.0033$). (**J**) Inhibition of CGRP^{PBN} neurons during visual US conditioning impaired the formation of auditory fear memory (RM two-way ANOVA, time × group, $F_{1,13} = 9.965$, $P = 0.0076$). (**K**) Schematic of optogenetic inhibition of CGRP^{PBN} neurons during auditory memory retrieval. (**L**) Inhibition of CGRP^{PBN} neurons impaired retrieval of auditory fear memory (eNpHR3.0, $N = 10$; EYFP, $N = 12$; RM two-way ANOVA, time × group, $F_{1,20} = 18.16$, $P = 0.0004$). All data are means ± SEM. $^*P < 0.05$, $^{**}P < 0.01$, $^{***}P < 0.001$, and $^{****}P < 0.0001$.

were identified in both the anterior IC (aIC) and posterior IC (pIC) in layers 5 and 6 (fig. S5, B and C), but projections from the pIC were notably denser (fig. S5D). Given that the pIC is more closely associated with pain and aversive states, whereas the aIC is primarily linked to appetitive processing (*54*–*56*), we focused on the pIC as a key candidate for relaying aversive affective signals. In the pIC, most green fluorescent protein–positive (GFP$^+$) cells showed clearly greater activation in the looming group than in the flickering group (Fig. 4, C and D, and fig. S5, A and B). Similarly, SC GFP$^+$ neurons in the intermediate layers exhibited increased activation to looming (Fig. 4, C and G). This pIC and SC-specific activation was restricted to GFP$^+$ projection neurons, as no group differences were found in GFP$^-$ populations across brain regions (Fig. 4, C to G). In contrast, no activation differences were observed in the CeA or PAG (Fig. 4,

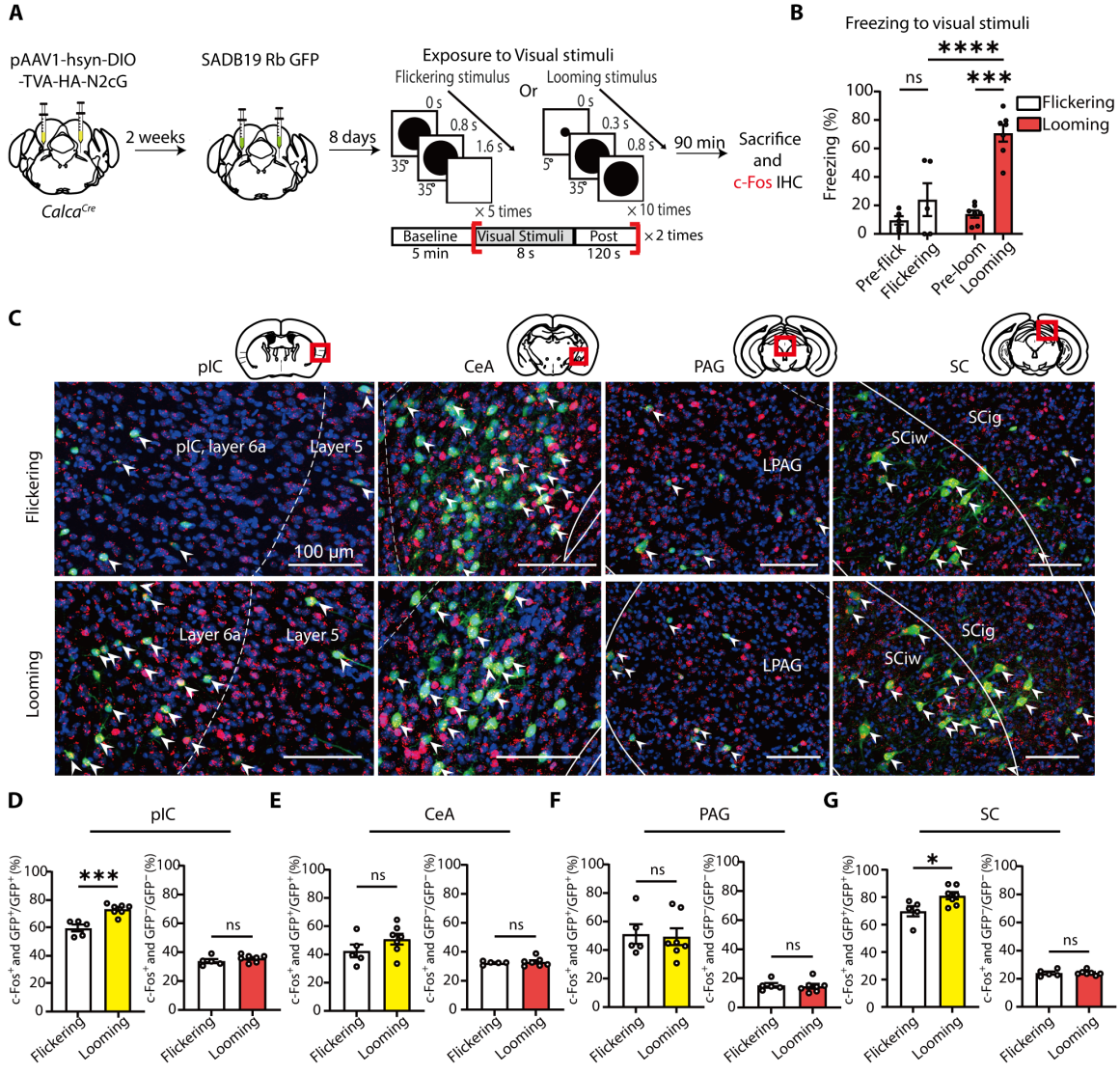

Fig. 4. Identification of CGRP^{PBN}-projecting neurons activated by looming visual stimuli. (**A**) Schematic of a monosynaptic retrograde tracing of CGRP^{PBN} neurons and c-Fos imaging in response to looming stimuli. Bilateral injections of AAV2/1-hsyn-DIO-TVA-HA-N2cG into the PBN of *Calca*^{Cre} mice were followed by bilateral injections of SADB19-GFP rabies virus into the same site. (**B**) Looming visual stimuli induced a robust freezing response in mice, whereas flickering stimuli did not (flickering, $N = 5$, looming, $N = 7$; RM two-way ANOVA, time × group, $F_{1,10} = 9.893$, $P = 0.0104$). (**C**) Representative confocal microscopic images showing CGRP^{PBN}-projecting GFP$^+$ neurons (green) and c-Fos$^+$ neurons (red) in the pIC, CeA, PAG, and SC. A white arrowhead indicates co-localized neurons. Images of starter cells in the PBN are presented in the fig. S4. Scale bars, 100 μm. LPAG, lateral PAG; SCiw, intermediate white layer of the SC; SCig, intermediate gray layer of the SC. (**D** to **G**) The ratio of double-positive neurons (GFP$^+$ and c-Fos$^+$) within GFP$^+$ or GFP$^-$ cell populations was compared between the groups (flickering versus looming) in each analyzed region: pIC (D) (flickering, $N = 5$; looming, $N = 7$; left; two-tailed unpaired *t* test, $t_{10} = 4.952$, $P = 0.0006$; right; $t_{10} = 1.145$, $P = 0.2787$), CeA (E) (left; $t_{10} = 1.404$, $P = 0.1906$; right; $t_{10} = 0.4580$, $P = 0.6567$), PAG (F) (left; $t_{10} = 0.2072$, $P = 0.8400$; right; $t_{10} = 0.2809$, $P = 0.7845$), and SC (G) (left; $t_{10} = 2.593$, $P = 0.0268$; right; $t_{10} = 0.1301$, $P = 0.8901$). All data are means ± SEM. *$P < 0.05$, ***$P < 0.001$, and ****$P < 0.0001$.

C, E, and F). These findings suggest that projection neurons in the pIC (pIC$^{\rightarrow CGRP\text{-}PBN}$) and SC are selectively activated by looming threats and may serve as upstream sources of US information for CGRP^{PBN} neurons.

Selective activation of pIC$^{\rightarrow CGRP\text{-}PBN}$ neurons in response to threat stimuli

The IC is well known for processing negative emotions and contributing to fear, anxiety, and disgust (*48*, *57*). In humans, IC activity correlates with affective and social pain, and lesions can lead to pain asymbolia, where pain is perceived without emotional distress (*48*, *58*–*60*). In rodents, optogenetic activation of the pIC induces an aversive state (*56*), and pIC activity is required for maintaining learned fear (*61*), suggesting its role in encoding aversive affect rather than sensory pain.

The IC has also been implicated in non-nociceptive fear conditioning. In humans, exposure to aversive images as a US increases IC activation in response to both the US and CS (*62*, *63*). In rodents, inactivation of the pIC impairs predator odor fear conditioning and memory recall (*15*). Notably, the IC has extensive reciprocal

connections with the PBN (*45*, *46*), and we identified the increased activity of pIC$^{\rightarrow CGRP\text{-}PBN}$ neurons in response to looming stimuli (Fig. 4D). Based on these findings, we hypothesized that the pIC transmits threat-relevant aversive affective signals to the CGRP^{PBN} neurons to drive visual threat conditioning.

To further prove whether pIC$^{\rightarrow CGRP\text{-}PBN}$ neurons selectively respond to threat stimuli, we performed photometry calcium recordings. Using a rabies virus–based Flp system, we expressed GCaMP6s selectively in pIC$^{\rightarrow CGRP\text{-}PBN}$ neurons (Fig. 5, A to C). Mice were exposed to either looming and foot shock stimuli or flickering and foot shock stimuli. Photometry recordings revealed that pIC$^{\rightarrow CGRP\text{-}PBN}$ neurons were persistently activated by both looming and foot shock stimuli but exhibited distinct activation dynamics: a slow increase to looming and a rapid increase to foot shock (Fig. 5, D to F). In contrast, flickering stimuli did not induce pIC$^{\rightarrow CGRP\text{-}PBN}$ activation, whereas foot shock elicited a robust response (Fig. 5, G to I). These findings indicate that pIC$^{\rightarrow CGRP\text{-}PBN}$ neurons selectively respond to threats rather than general sensory stimuli.

Moreover, the sustained activity of pIC$^{\rightarrow CGRP\text{-}PBN}$ neurons beyond threat exposure suggests they encode persistent aversive states rather than transient threat detection (*56*, *64*, *65*). Their prolonged response to looming stimuli also parallels the sustained activation observed in CGRP^{PBN} neurons (Fig. 2D), suggesting that pIC input may contribute to prolonged CGRP^{PBN} activation.

pIC$^{\rightarrow PBN}$ neurons are required for CGRP^{PBN} neuronal activation by visual threats but not to foot shock

If the pIC transmits threat-relevant signals to CGRP^{PBN} neurons, then its input should be required for CGRP^{PBN} activation. To test this, we inhibited pIC neurons projecting to the PBN (pIC$^{\rightarrow PBN}$) using DREADDs (designer receptors exclusively activated by designer drugs) while monitoring CGRP^{PBN} activity in response to looming and foot shock. Cre-dependent AAV-hsyn-DIO-GCaMP6m was injected into the PBN of *Calca*^{Cre} mice, and an optic fiber was implanted above the injection site (Fig. 6A). To selectively express hM4Di DREADDs in pIC$^{\rightarrow PBN}$ neurons, AAVretro-FlpO was injected into the PBN, followed by Flp-dependent AAV encoding hM4Di-mCherry (or mCherry as a control) into the pIC (Fig. 6B).

Compound 21 (C21), a DREADD agonist (*66*), was administered 1 hour before photometry recordings to inhibit pIC$^{\rightarrow PBN}$ neurons. In response to looming stimuli, CGRP^{PBN} activation was distinctly reduced in the hM4Di group compared to controls (Fig. 6, C to F), with a persistent suppression lasting over 1 min (Fig. 6G). By contrast, CGRP^{PBN} neurons in the hM4Di group responded normally to foot shock (Fig. 6, H to L). These findings indicate that pIC input is required for looming-induced CGRP^{PBN} activation but not for foot-shock responses. Given the pIC's primary role in processing aversive affect, the absence of pIC$^{\rightarrow PBN}$ input during foot shock may be compensated by alternative nociceptive pathways, such as those involving the spinal cord or PAG.

Further axon tracing of pIC$^{\rightarrow PBN}$ neurons (fig. S6) revealed projections to multiple brain regions, including the CeA, basomedial amygdalar nucleus, parasubthalamic nucleus, posterior thalamic regions, and PAG—key areas in emotional regulation and learning (*39*, *67*–*70*). This suggests that pIC$^{\rightarrow PBN}$ neurons encode aversive states and broadly relay this information to coordinate behavioral and physiological responses. The observed collateral projections imply that pIC$^{\rightarrow PBN}$ input contributing to CGRP^{PBN} neuronal responses to looming stimuli may be relayed either directly or indirectly through other regions.

pIC-to-PBN pathway is necessary for visual threat conditioning but not for foot-shock conditioning

Since pIC$^{\rightarrow PBN}$ neurons are essential for CGRP^{PBN} activation by visual threats, we tested whether the direct pIC-to-PBN pathway is required for visual threat conditioning. To inhibit this pathway during conditioning, we injected AAV encoding eNpHR3.0-EYFP [or enhanced GFP (EGFP) as a control] into the bilateral pIC and implanted optic fibers above the PBN (Fig. 7, A and B). Optogenetic inhibition during visual threat conditioning did not alter immediate freezing but impaired fear memory formation (Fig. 7, C and D). While control mice exhibited a marked increase in freezing to the tone CS during retrieval, eNpHR3.0-expressing mice showed no no observable change.

Next, we examined whether the pIC-PBN pathway is necessary for foot-shock conditioning. For foot-shock conditioning, a 20-s tone CS was presented, with the last 2 s paired with a 0.5-mA foot shock (Fig. 7, E and F). This tone-shock pairing was repeated five times while inhibiting pIC-PBN terminals during conditioning. Optogenetic inhibition did not affect defensive escape behavior elicited by the foot shock (Fig. 7G). However, unlike visual threat conditioning, inhibition of pIC-PBN pathway had no effect on foot-shock conditioning (Fig. 7H). These results indicate that the pIC-PBN pathway serves as a selective US pathway for visual threat conditioning rather than foot-shock conditioning.

Last, given the sustained responses of both pIC and CGRP^{PBN} neurons to looming stimuli, we investigated the precise timing at which pIC input is required for visual threat conditioning. We selectively inhibited the pIC→PBN pathway either strictly during US exposure or during the ITI (Fig. 7, I and J). Inhibition during US exposure had no effect on conditioned freezing (Fig. 7I). However, inhibition during the ITI impaired fear memory formation—control mice exhibited increased freezing to the tone CS, whereas eNpHR3.0-expressing mice did not (Fig. 7J). These results show that sustained pIC→PBN input is critical for visual threat conditioning, while transient input during US exposure alone is insufficient. Overall, these findings suggest that pIC neurons provide essential, persistent input to the PBN for visual threat conditioning but are not required for foot-shock conditioning, consistent with our photometry results (Fig. 6).

pIC$^{\rightarrow CGRP\text{-}PBN}$ projections to the PBN induce aversive behavioral states and drive threat conditioning as a US

Our data indicate that the pIC-to-PBN circuit functions as a US pathway for visual threat conditioning. As we hypothesized that this pathway transmits aversive affective information, we examined whether direct activation of the circuit induces aversive affective states and is sufficient to drive threat conditioning. For this purpose, we targeted pIC$^{\rightarrow CGRP\text{-}PBN}$ neurons with channelrhodopsin-2 (ChR2) and optically stimulated their axon terminals in the PBN (Fig. 8A). Cre-dependent AAV was injected into the bilateral PBN of *Calca*^{Cre} mice, and Flp-dependent AAV encoding ChR2–enhanced yellow fluorescent protein (EYFP) (or EYFP alone) was injected into the bilateral pIC. Two weeks later, rabies virus encoding Flp recombinase fused with mCherry was injected into the PBN at the same viral injection sites. Post hoc histological analysis confirmed specific ChR2 expression in pIC neurons, coexpressed with Flp-mCherry (Fig. 8B). Starter cells were detected exclusively in the PBN (fig. S4B). To assess aversive behaviors, we conducted the real-time place avoidance (RTPA), open-field test (OFT), and elevated plus maze (EPM) tests.

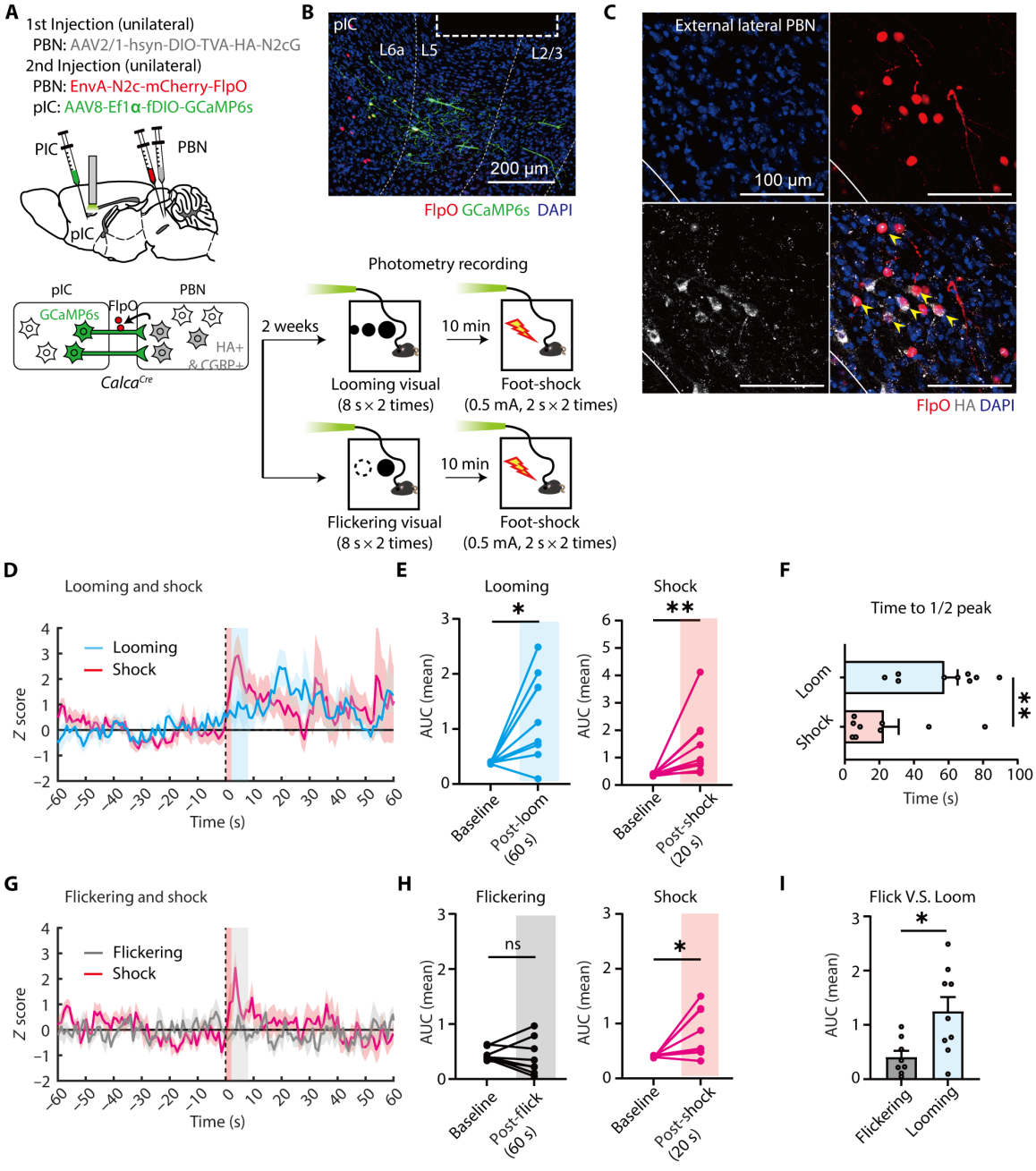

Fig. 5. Fiber photometry recordings of pIC$^{\rightarrow CGRP\text{-}PBN}$ neuronal activity in response to visual and foot-shock stimuli. (**A**) Schematic of fiber photometry recordings of pIC$^{\rightarrow CGRP\text{-}PBN}$ neuronal responses to looming (or flickering) and foot-shock stimuli. (**B**) Representative image of GCaMP6s (green) and FlpO (red) expression in the pIC. All GCaMP6s^{+} cells were FlpO^{+}. The dotted rectangle marks the optic fiber location. Scale bar, 200 μm. (**C**) Representative images of starter cells in the PBN. Yellow arrowheads indicate FlpO-mCherry^{+} and HA^{+} starter cells. Scale bars, 100 μm. (**D**) *z*-scored calcium activity (means ± SEM) in response to looming and foot-shock stimuli (the blue shaded area: 8-s looming stimuli; the red shaded area: 2-s foot shock). (**E**) Average during looming and foot-shock ($N = 9$ mice; left; baseline = −60 to 0 s, looming = 0 to 60 s after the onset of visual stimuli; Two-tailed paired *t* test, $t_8 = 3.291$, $P = 0.011$; right; shock = 0 to 20 s after the onset of shock stimuli; two-tailed Wilcoxon matched pairs signed-rank test, $W = 45$, $P = 0.0039$). (**F**) Time to reach half of the peak *z* score after the peak (two-tailed Mann-Whitney test, $U = 11$, $P = 0.0072$). (**G**) *z*-scored calcium activity (means ± SEM) during flickering and foot shock (the gray shaded area: 8-s flickering stimuli; the red shaded area: 2-s foot shock). (**H**) Average AUC during flickering and foot shock ($N = 8$ mice; left; baseline = −60 to 0 s, flickering = 0–60 s after the onset of visual stimuli; Two-tailed Wilcoxon matched pairs signed-rank test, $W = -6$, $P = 0.7422$; right; shock = 0–20 s after the onset of shock stimuli; two-tailed paired *t* test, $t_7 = 2.791$, $P = 0.0269$). (**I**) Comparison of AUC between flickering and looming (two-tailed unpaired *t* test, $t_{15} = 2.798$, $P = 0.0135$). All data are presented as means ± SEM. *$P < 0.05$ and **$P < 0.01$.

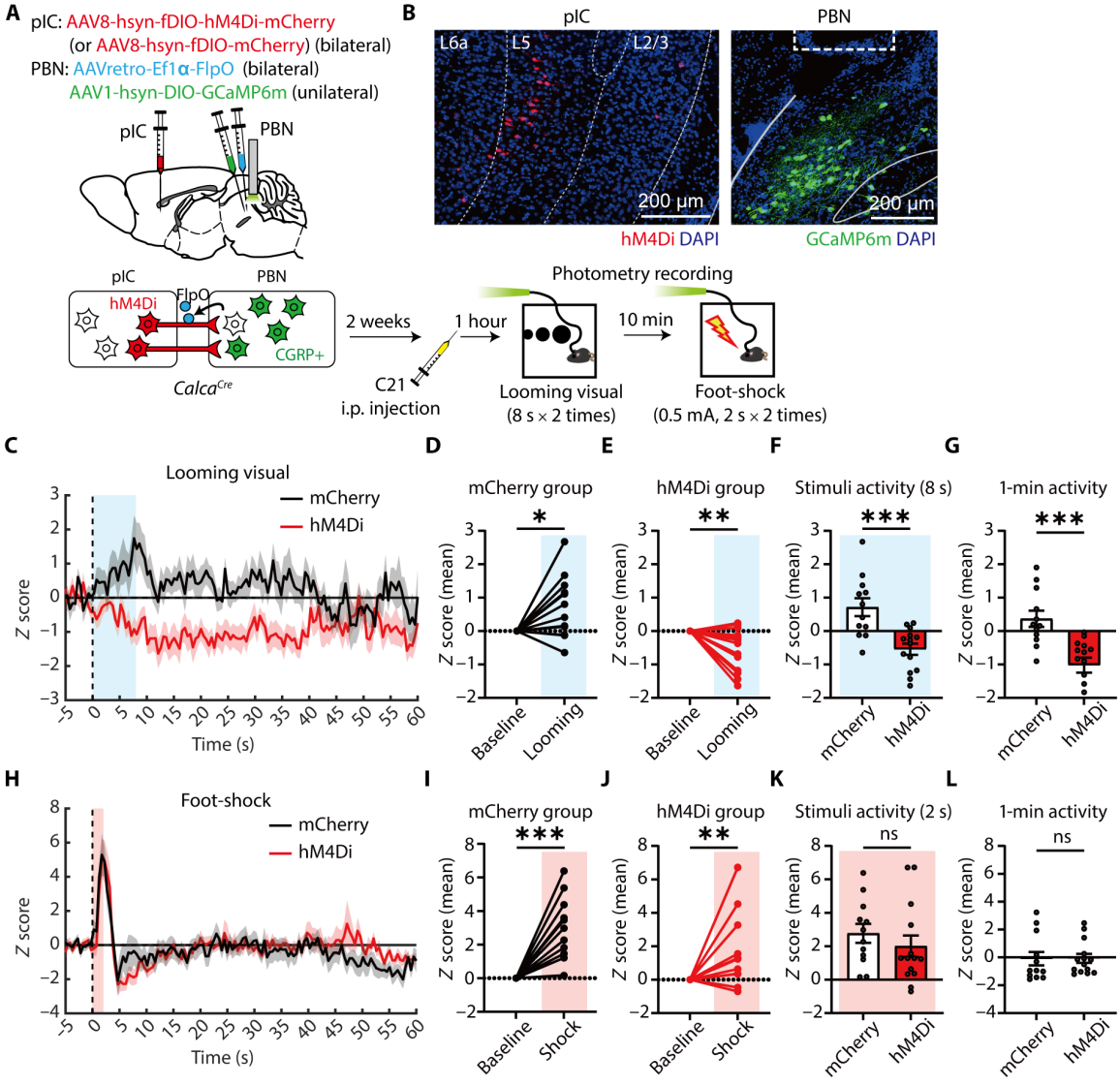

Fig. 6. pIC$^{\rightarrow PBN}$ neurons are necessary for activation of CGRP^{PBN} neurons to looming but not foot-shock stimuli. (**A**) Schematic of photometry recording of CGRP^{PBN} neurons with hM4Di inhibition of pIC$^{\rightarrow PBN}$ neurons. (**B**) Representative images showing expression of hM4Di-mCherry in the pIC$^{\rightarrow PBN}$ neurons (left) and GCaMP6m in CGRP^{PBN} neurons (right). The dotted rectangle indicates the location of optic fiber. Scale bars, 200 μm. (**C**) *z*-scored calcium activities of CGRP^{PBN} neurons to visual stimuli (blue shaded area: 8-s looming stimuli). (**D** and **E**) Average calcium activity during visual stimuli in the mCherry group (D) (baseline = −5 to 0 s, looming = 0 to 8 s; $N = 12$ trials; two trials per mouse, six mice; one sample *t* test, $t_{11} = 2.659$, $P = 0.0222$) and hM4Di group (E) ($N = 14$ trials; two trials per mouse, seven mice; $t_{13} = 3.266$, $P = 0.0061$). (**F** and **G**) Comparison of average changes in calcium activity evoked by looming stimuli between two groups during stimuli (F) (two-tailed unpaired *t* test, $t_{24} = 4.104$, $P = 0.0004$) and for 1 min (G) (two-tailed unpaired *t* test, $t_{24} = 4.203$, $P = 0.0003$). (**H**) *z*-scored calcium activities of CGRP^{PBN} neurons to foot-shock stimuli (red shaded area: 2-s foot shock). (**I** and **J**) Average calcium activity during foot-shock in the mCherry group (I) (baseline = −5 to 0 s, shock = 0 to 2 s; $N = 12$ trials; one sample *t* test, $t_{11} = 4.887$, $P = 0.0005$) and hM4Di group (J) ($N = 14$ trials; one sample Wilcoxon test, $W = 89$, $P = 0.0031$). (**K** and **L**) Comparison of average changes in calcium activity evoked by foot-shock stimuli between two groups during stimuli (K) (two-tailed Mann-Whitney test, $U = 63$, $P = 0.2972$) and for 1 min (L) (two-tailed Mann-Whitney test, $U = 69$, $P = 0.4624$). All data are means ± SEM. *$P < 0.05$, **$P < 0.01$, and ***$P < 0.001$.

In the RTPA test, mice were placed in a three-chamber arena where one side was paired with photostimulation of pIC$^{\rightarrow CGRP\text{-}PBN}$ axon terminals in the PBN. The EYFP control group showed no preference between chambers, whereas the ChR2 group avoided the light-paired chamber (Fig. 8, C to F). In the OFT, photostimulation was alternated with 60-s intervals (Fig. 8, G and H). The ChR2 group did not exhibit increased freezing, suggesting that pIC$^{\rightarrow CGRP\text{-}PBN}$ activation does not induce freezing behavior (Fig. 8, H and I). However, ChR2 mice showed increased anxiety, spending less time in the center zone and crossing it fewer times than controls despite similar total movement distance (Fig. 8, J to L). In the EPM test, light stimulation was alternated (2-s on, 2-s off) throughout the trial. ChR2 group spent more time in the closed arms compared to EYFP controls (Fig. 8O). Although not statistically significant, they also showed a tendency to spend less time in the open arms (Fig. 8N). In addition, the number of open arm entries was substantially decreased in the ChR2 group (Fig. 8P), while total movement distance remained comparable between groups (Fig. 8R). These results suggest that activation

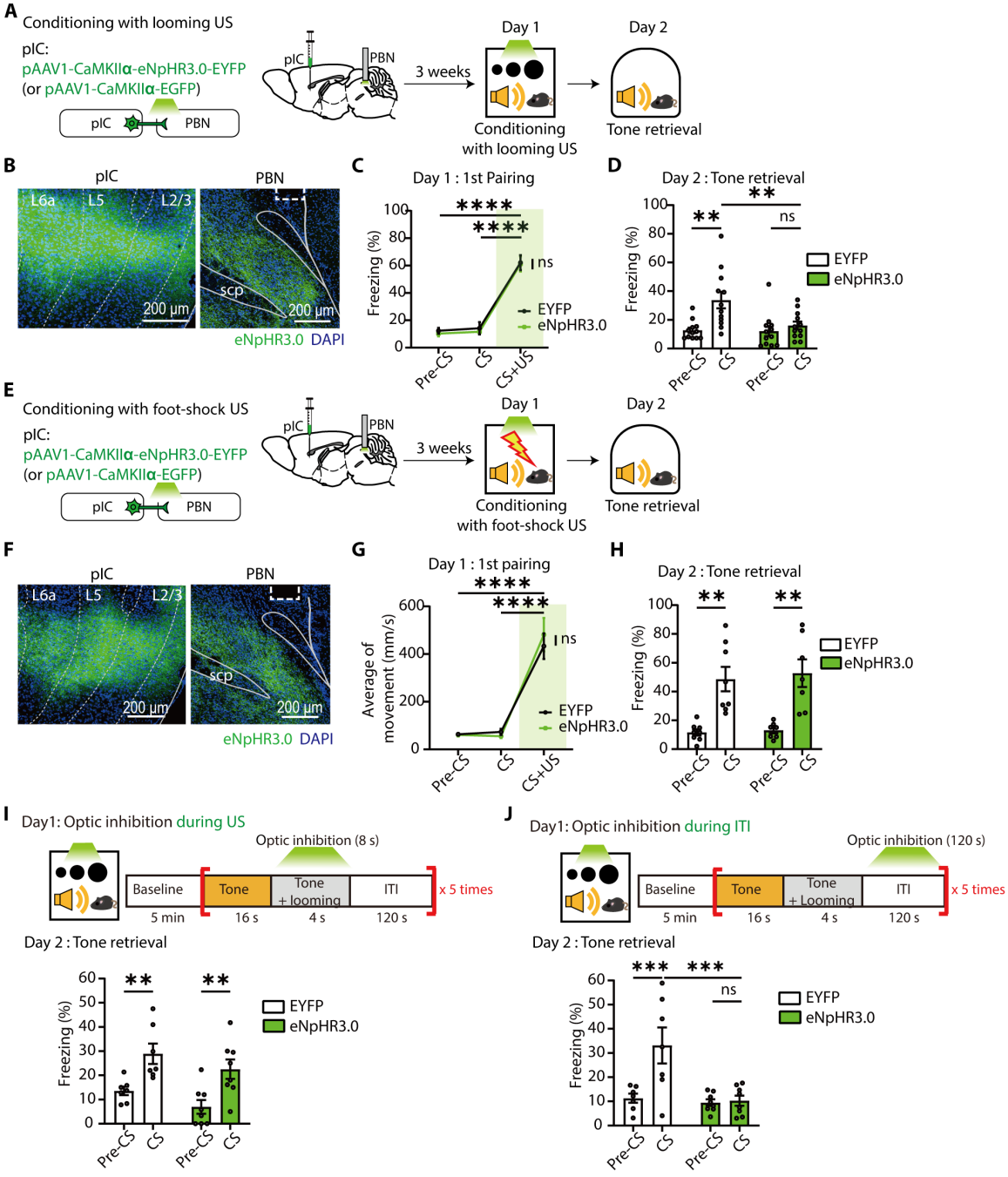

Fig. 7. pIC projections to the PBN are required for threat conditioning with looming but not with foot-shock stimuli. (**A**) Schematic of optogenetic inhibition of pIC-PBN circuit during visual threat conditioning. (**B**) Representative images of eNpHR3.0-EYFP expression in pIC neurons (left) and their axons in the PBN (right). Dotted rectangle indicates optic fiber tip. Scale bars, 200 μm. (**C**) Freezing levels during first CS-US pairing (EYFP, $N = 12$; eNpHR3.0, $N = 12$; RM two-way ANOVA, time, $F_{2,44} = 125.6$, $P < 0.0001$). (**D**) Inhibition of pIC-PBN projections during conditioning impaired auditory fear memory formation (RM two-way ANOVA, time × group, $F_{1,22} = 4.550$, $P = 0.0443$). (**E** and **F**) Schematic and representative images of pIC-PBN inhibition during foot-shock conditioning. The dotted rectangle marks the optic fiber tip. Scale bars, 200 μm. (**G**) Average of movement during the first pairing of tone CS and foot-shock US on day 1 (EYFP, $N = 8$; eNpHR3.0, $N = 7$; RM two-way ANOVA, time, $F_{2,26} = 71.34$, $P < 0.0001$). (**H**) Inhibition of pIC-PBN projections during foot-shock conditioning did not affect the formation of fear memory (RM two-way ANOVA, time, $F_{1,13} = 30.91$, $P < 0.0001$). (**I**) Optogenetic inhibition of pIC-PBN projections during US exposure (2 s before to 2 s after US; total 8 s) did not impair auditory fear memory formation (EYFP, $N = 7$; eNpHR3.0, $N = 8$; RM two-way ANOVA, time, $F_{1,13} = 38.2$, $P < 0.0001$). (**J**) Optogenetic inhibition of pIC axon terminals in the PBN during ITI impaired auditory fear memory formation (EYFP, $N = 7$; eNpHR3.0, $N = 8$; RM two-way ANOVA, time × group, $F_{1,13} = 12.76$, $P = 0.0034$). All data are means ± SEM. $^{**}P < 0.01$, $^{***}P < 0.001$, and $^{****}P < 0.0001$.

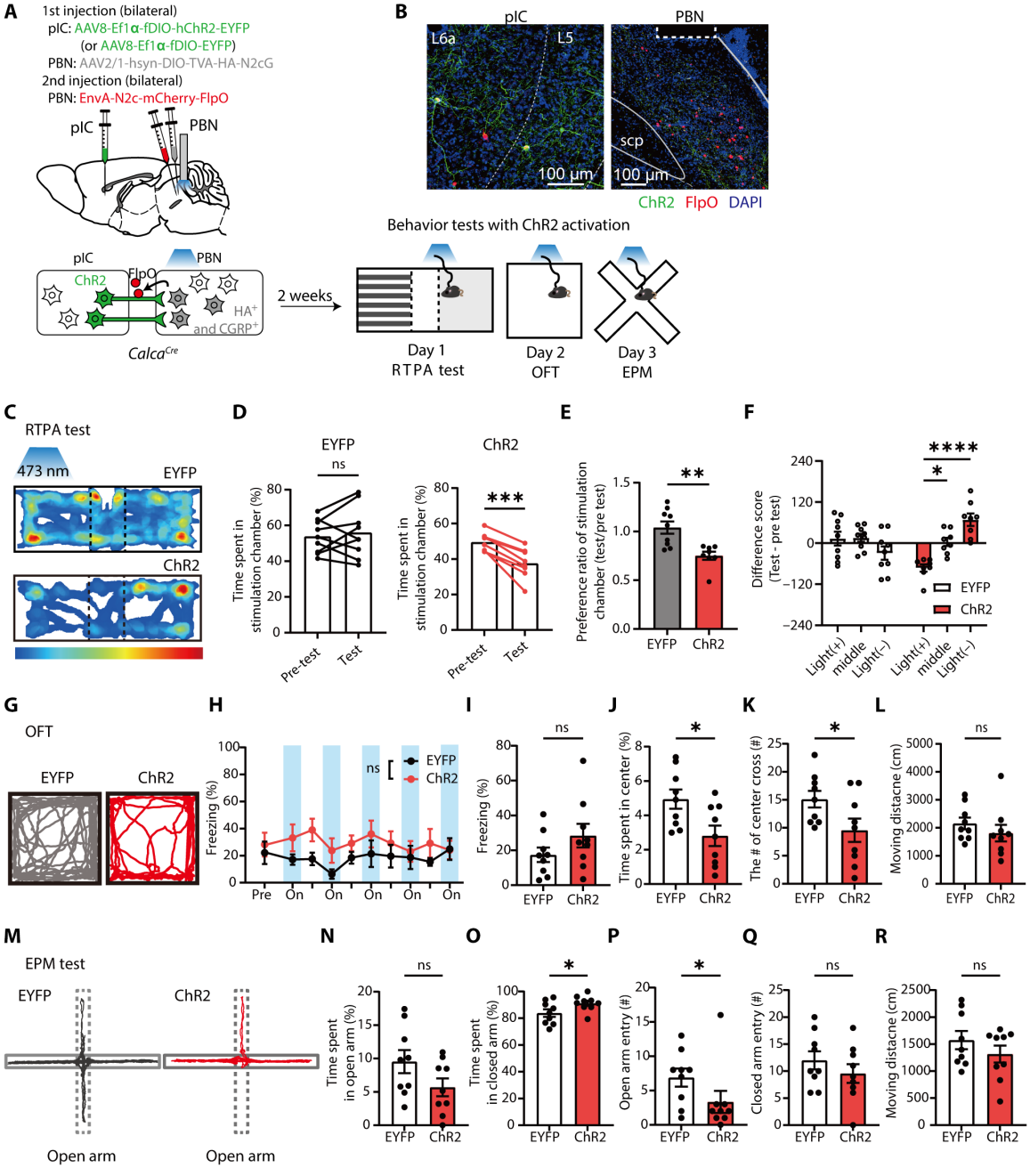

Fig. 8. Optogenetic stimulation of pIC$^{\rightarrow CGRP\text{-}PBN}$ projections induces anxiogenic behaviors. (**A**) Schematic of viral injections and behavior tests. (**B**) Representative images of ChR2 (green) and/or retrogradely labeled FlpO (red) expression in the pIC (left) and PBN (right). The dotted rectangle marks the optic fiber location. (**C**) Representative heatmaps of time spent in RTPA test chambers during photostimulation. (**D** to **F**) ChR2 group avoided the photostimulated-paired chamber. (D) Time spent in the photostimulated chamber (left, EYFP; $N = 9$; two-tailed paired t test, $t_8 = 0.6490$, $P = 0.5345$; right, ChR2; $N = 8$, $t_7 = 6.837$, $P = 0.0002$). (E) Preference ratio for the photostimulated chamber (two-tailed Mann-Whitney test, $U = 6$, $P = 0.0025$). (F) Difference score for each chamber (RM two-way ANOVA, time × group, $F_{2,30} = 10.77$, $P = 0.0003$). (**G**) Representative movement trajectory during the OFT. (**H** to **L**) ChR2 photostimulation increased anxiety-like behaviors. (H) Photostimulation did not induce a freezing (EYFP, $N = 9$; ChR2, $N = 9$; RM two-way ANOVA, time × group, $F_{9,144} = 0.8810$, $P = 0.5439$). Averages of freezing levels (I) (Two-tailed unpaired t test, $t_{16} = 1.379$, $P = 0.1870$), time spent in the center zone (J) ($t_{16} = 2.627$, $P = 0.0183$), number of center zone crossings (K) ($t_{16} = 2.167$, $P = 0.0456$), and moving distance (L) ($t_{16} = 1.131$, $P = 0.2748$). (**M**) Representative movement trajectory during EPM. (**N** to **R**) Time spent in open arms (N) (EYFP, $N = 9$; ChR2, $N = 9$; $t_{16} = 1.406$, $P = 0.0894$), time spent in closed arms (O) ($t_{16} = 2.141$, $P = 0.0480$), open arm entries (P) (U = 18.5, $P = 0.0495$), closed arm entries (Q) ($t_{16} = 1.012$, $P = 0.3267$), and moving distance (R) ($t_{16} = 1.129$, $P = 0.2757$). Two-tailed Mann-Whitney test in (P) and two-tailed unpaired t test in [(N), (O), (Q), and (R)] were used. All data are means ± SEM. *$P < 0.05$, **$P < 0.01$, ***$P < 0.001$, and ****$P < 0.0001$.

of pIC$^{\rightarrow CGRP\text{-}PBN}$ projections in the PBN induces aversive affective behavioral states.

We next examined whether photostimulation of pIC$^{\rightarrow CGRP\text{-}PBN}$ projections in the PBN can serve as a US to drive threat conditioning. Using the same viral strategy, we selectively expressed ChR2 in pIC$^{\rightarrow CGRP\text{-}PBN}$ neurons (Fig. 9, A and B, and fig. S4C). During conditioning, photostimulation of these projections in the PBN was paired with the tone CS five times. In the tone retrieval test, only the ChR2 group exhibited increased freezing to the tone CS compared to the pre-CS period, while the EYFP control group did not (Fig. 9C). These findings demonstrate that pIC$^{\rightarrow CGRP\text{-}PBN}$ neurons transmit aversive affective information to the PBN and that this pathway is sufficient to drive threat conditioning, revealing a distinct circuit for threat learning.

DISCUSSION

In this study, we established a visual threat conditioning model using looming stimuli as a US in mice. We demonstrated that CGRP^{PBN} neurons are essential for visual threat conditioning and play a broader role in fear learning across both nociceptive and non-nociceptive US. In addition, we identified a distinct top-down pIC→CGRP^{PBN} circuit as a critical aversive US pathway required for visual threat conditioning. Both pIC$^{\rightarrow CGRP\text{-}PBN}$ and CGRP^{PBN} neurons exhibited threat-specific responses, and the pIC-PBN circuit was necessary for visual threat conditioning but dispensable for foot-shock conditioning. Moreover, activation of pIC$^{\rightarrow CGRP\text{-}PBN}$ projections in the PBN induced aversive affective states and was sufficient to drive fear memory formation. Given the monosynaptic connectivity between pIC and CGRP^{PBN} neurons, these findings suggest that the pIC→CGRP^{PBN} pathway functions as a primary US pathway for non-nociceptive danger signals.

CGRP^{PBN} neurons as a hub for threat assessment and fear learning

CGRP^{PBN} neurons integrate external and internal signals for comprehensive threat assessment, acting as a general danger-detection hub (*38*, *39*, *51*). They selectively respond to threats such as looming and foot shock but not to neutral stimuli (Figs. 2 and Fig. 6), highlighting their role in associative fear learning. After conditioning, their responses to the tone CS increased (Fig. 2, M to O), suggesting synaptic plasticity enables encoding of learned danger. Both inactivation of CGRP^{PBN} neurons during conditioning and retrieval impaired conditioned freezing (Fig. 3, G to L), indicating their necessity for both fear memory formation and recall, reinforcing their central role in visual threat conditioning.

Distinct pIC-PBN pathway in encoding aversive states

We found that the pIC-PBN pathway transmits aversive affective signals crucial for visual threat conditioning. The pIC$^{\rightarrow CGRP\text{-}PBN}$ neurons selectively respond to both visual and foot-shock threats, but not to neutral stimuli such as flickering (Fig. 5), highlighting their role in processing aversive rather than neutral sensory input. Consistent with this, human studies show that the insula is involved in both nociceptive and psychological distress (*58*, *59*). These findings suggest that pIC$^{\rightarrow CGRP\text{-}PBN}$ neurons may constitute a specific population that conveys affective pain signals from multimodal sensory inputs to the PBN. In addition, optogenetic activation of the pIC$^{\rightarrow CGRP\text{-}PBN}$ pathway induced an aversive state and drove fear memory formation in mice, reinforcing its role in encoding aversive affect (Figs. 8 and 9).

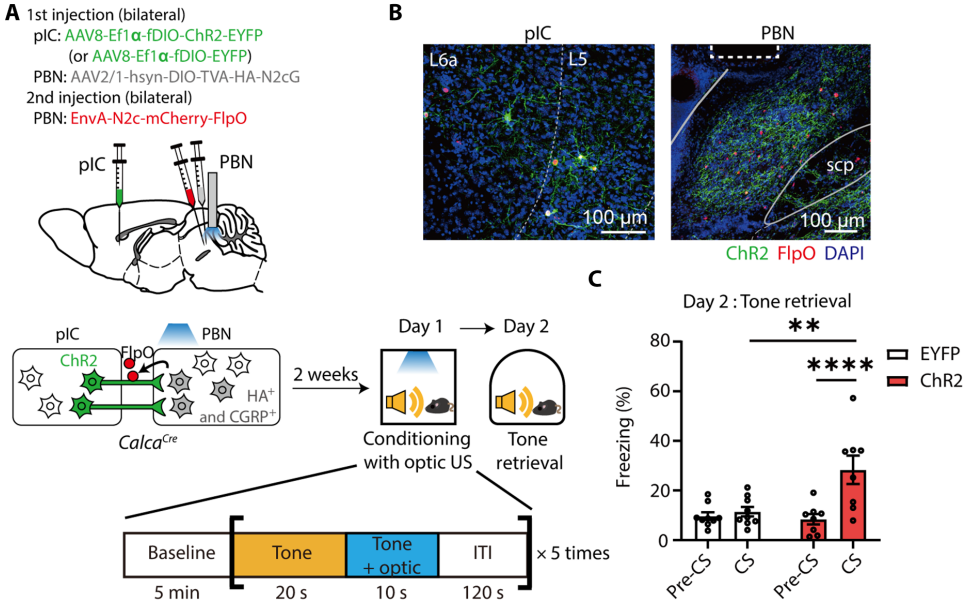

Fig. 9. Optogenetic stimulation of pIC$^{\rightarrow CGRP\text{-}PBN}$ projections is sufficient to drive formation of fear memory. (**A**) Schematic of a threat conditioning paradigm with optogenetic stimulation of pIC$^{\rightarrow CGRP\text{-}PBN}$ projections as s a US. During conditioning, mice were exposed to a 30-s tone, during which the last 10-s tone presentation was overlapped with optic stimulation. This CS-US pairing was repeated five times at a 120-s interval. (**B**) Representative images showing the neurons expressing ChR2 (green) and/or retrograde labeled FlpO (Red) in the pIC (left) and ChR2-expressing neurons projections (green) in the PBN (right). Neurons expressing FlpO were also detected in the PBN (right). The dotted rectangle indicates the location of the optic fiber. Scale bars, 100 μm. (**C**) ChR2-expressing mice exhibited increased freezing levels to the conditioned tone during the fear memory retrieval test (EYFP, $N = 9$; ChR2, $N = 8$; RM two-way ANOVA, time × group, $F_{1,15} = 15.22$, $P = 0.0014$). All data are means ± SEM. $^{**}P < 0.01$ and $^{****}P < 0.0001$.

Inhibition of the pIC-PBN pathway during the ITI impaired fear memory formation (Fig. 7J), suggesting that sustained input from the pIC to PBN is required for visual threat conditioning. This prolonged pIC activity may be maintained by interoceptive inputs from physiological changes induced by threats. Activation of SC parvalbumin-positive (PV^+) neurons, which receive direct visual input from retinal ganglion cells (RGCs) and selectively respond to looming threats, increases heart rate (*71*), and $CGRP^{PBN}$ neurons contribute to tachycardia and anxiety-like behaviors (*72*). Given the role of pIC in bottom-up cardiac interoceptive processing (*73*), physiological signals may help maintain long-lasting pIC activity. Alternatively, local recurrent connectivity, involving fast feedback inhibition and slow neuromodulatory transmission (*74*, *75*) or bidirectional interactions with the PBN (*45*, *46*), could contribute to prolonged activation.

In contrast, the pIC-PBN circuit was not essential for foot-shock conditioning (Fig. 7H). In addition, silencing $pIC^{\rightarrow PBN}$ neurons disrupted $CGRP^{PBN}$ responses to looming but not to foot shock (Fig. 6), suggesting that visual threats, which lack sensory pain, primarily engage the pIC for aversive processing. Meanwhile, foot shocks, which involve both affective and sensory pain, can recruit alternative pathways such as the spinal cord and PAG to activate $CGRP^{PBN}$ neurons and support fear learning.

Dissociating innate defensive responses from learned fear

A critical distinction in our study is the separation of innate defensive responses and fear learning processes. $CGRP^{PBN}$ neurons were required for threat conditioning and learned fear responses but not for immediate defensive behaviors to visual threats (Fig. 3D and fig. S2). This aligns with studies showing that $CGRP^+$ neurons in the thalamic parvocellular subparafascicular nucleus ($CGRP^{SPFp}$), rather than $CGRP^{PBN}$ neurons, mediate innate freezing to looming threats (*39*). $CGRP^{PBN}$ neurons are required for innate freezing in response to other threat modalities, such as loud tones (*39*), suggesting a modality-specific dissociation in defensive behaviors. Looming stimuli, which mimic fast-approaching objects, likely elicit rapid, reflex-like reactions, whereas fear learning requires a slower risk-assessment process mediated by the PBN.

The SC is a key structure in processing looming threats and coordinating immediate defensive responses. SC PV^+ neurons receive direct input from RGCs and specifically respond to looming threats. In addition, SC neurons transmit looming-relevant inputs to multiple brain regions, including the PBGN, LPTN, PAG, and VTA, which regulate immediate escape and freezing responses (*43*, *44*, *71*, *76*, *77*). Thus, an SC-derived visual pathway, independent of $CGRP^{PBN}$ neurons, is likely responsible for mediating looming-induced innate freezing.

The presumed role of the SC-PBN pathway in visual threat processing

Although we did not directly assess the function of the SC-PBN pathway, c-Fos analysis revealed increased activity in $SC^{\rightarrow CGRP\text{-}PBN}$ neurons in response to looming stimuli. Since SC neurons detect specific looming patterns in the visual field, the SC-PBN pathway may rapidly transmit potential threat-related visual information to the PBN. It is also possible that SC-PBN pathway is upstream of initial activation of $pIC^{\rightarrow CGRP\text{-}PBN}$ neurons, either directly or via intermediary structures. Given that $pIC^{\rightarrow CGRP\text{-}PBN}$ neurons show increased activity during threat exposure (Fig. 5), the pIC likely receives visual threat information rapidly. However, because the retina and SC lack known direct projections to the pIC, visual signals may be relayed from the SC to the pIC via the PBN. Alternatively, the pIC may receive threat-related signals from other intermediary structures such as the thalamus and amygdala.

The functional role of SC-PBN in fear learning remains unknown. Future studies should investigate the SC-PBN pathway's role in visual threat conditioning and clarify where the neural circuits for innate freezing and threat conditioning diverge.

Comparison to previous studies and unresolved questions

A prior study reported a failure to achieve Pavlovian fear conditioning with looming stimuli in rats (*78*), which differs from our findings in mice. This discrepancy may stem from differences in experimental conditions, particularly the strong food drive present in the prior study. $CGRP^{PBN}$ neurons integrate both hunger and danger signals, and their suppression by hunger-related inputs (*79*, *80*) may have interfered with aversive learning. The prior study found that combining looming with foot shock successfully impaired food retrieval behavior, suggesting complementary roles for these stimuli in recruiting fear-learning circuits. Future studies should explore how $CGRP^{PBN}$ neurons receive distinct inputs for different types of threats and how their activity is modulated by physiological states.

Future research should examine whether the pIC-PBN circuit serves as a general US circuit for non-nociceptive threats or is specific to visual stimuli. In addition, identifying the downstream targets of the pIC-PBN circuit responsible for mediating aversive states and associative learning will be crucial. Because the fiber photometry approach lacks single-cell resolution, it remains unclear whether individual $pIC^{\rightarrow PBN}$ and $CGRP^{PBN}$ neurons respond to both visual and tactile inputs or if distinct subpopulations exist for each modality. Given the role of $CGRP^{PBN}$ neurons in integrating affective signals, investigating the human homologs of this circuit could provide valuable insights into therapeutic targets for anxiety and fear-related disorders.

Our findings reveal a top-down circuit mechanism by which non-nociceptive visual stimuli induce aversive behavioral states and drive fear memory formation. Identifying this distinct fear memory circuit broadens our understanding of how environmental threats shape fear memory and may inform treatments for threat-related neuropsychiatric disorders, including PTSD.

MATERIALS AND METHODS

Mouse strains

Adult (8 to 24 weeks) C57BL/6J and heterozygous $Calca^{Cre}$ (C57BL/6J) mice were used for experiments. Heterozygous $Calca^{Cre}$ mice were generated by crossing homozygote $Calca^{Cre}$ mice (JAX, #033168) and C57BL/6J wild-type mice. Both male and female mice were used in balance, as we did not observe any noticeable differences in behaviors between male and female. Mice were group housed (three to five mice per cage) under a 12-hour light/12-hour dark cycle at a constant humidity (40 to 60%) and temperature (20° to 24°C). Food and water were available ad libitum. All procedures and protocols were approved by the KAIST Institutional Animal Care and Use Committee (KAIST IACUC, protocol # KA2020-16). All experiments were performed in accordance with the guideline of the KAIST IACUC.

Viruses

AAV1-hSyn-DIO-TeTox-P2A-nls-dTomato [5×10^{12} viral genome (vg)/ml], AAV1-hSyn-DIO-tdTomato (8×10^{11} vg/ml), AAV1-Ef1α-DIO-eNpHR3.0-EYFP (1×10^{12} vg/ml), AAV1-CaMKIIα-eNpHR3.0-EYFP (2.5×10^{12} vg/ml), AAV1-CaMKIIα-EGFP (2×10^{12} vg/ml), AAV8-hSyn-fDIO-mCehrry (8×10^{11} vg/ml), AAV8-Ef1α-fDIO-hChR2-EYFP (5×10^{13} vg/ml), and AAV8-Ef1α-fDIO-EYFP (3×10^{13} vg/ml) were packaged.

AAV1-Ef1α-DIO EYFP (2×10^{13} vg/ml), AAV8-hSyn-fDIO-hM4Di-mCehrry (2.5×10^{13} vg/ml), AAVretro-Ef1α-FlpO (2.3×10^{13} vg/ml), AAV1-hsyn-DIO-GCaMP6m (1.9×10^{13} vg/ml), AAV8-Ef1α-fDIO-GCaMP6s (1.3×10^{13} vg/ml), and AAV1-Ef1α-DIO-FlpO (2.1×10^{13} vg/ml) were purchased from Addgene. AAVdj-hsyn-fDIO-mGFP-2A-Synaptophysin-mRuby (1.9×10^{12} vg/ml) was purchased from Stanford gene vector and virus core.

The helper and rabies viruses were obtained from the Viral Vector Core facility of the Kavli Institute for Systems Neuroscience, Norwegian University of Science and Technology. The titers of each virus are as follows: AAV-hsyn-DIO-TVA-HA-N2cG (5×10^{11} vg/ml), EnvA pseudotyped SADB19 Rb GFP (1×10^{11} vg/ml), and EnvA pseudotyped N2c Rb-mCherry-FlpO (4.4×10^{8} vg/ml). The helper virus was diluted to 5×10^{10} vg/ml in sterile Dulbecco's phosphate-buffered saline (DPBS) (Gibco, Thermo Fisher Scientific) before use for a specific Cre-dependent avian tumor virus receptor A (TVA) expression as recommended by a previous paper (*81*).

Virus packaging

Adeno-associated virus (AAV) was packaged as previously described (*82*). The AAV DNA vector constructs used in this study were either obtained by subcloning of plasmids or purchased from addgene. Briefly, we amplified and purified DNA plasmid by using Maxiprep kit (QIAGEN). The prepared DNA vector was cotransfected with the viral vector (pAd ΔF6 and AAV2/1 or AAV2/8) into human embryonic kidney–293T cells (American Type Culture Collection, #CRL-3216) by using calcium phosphate precipitation. Seventy-two hours after transfection, cells were harvested, and virus was purified on iodixanol gradient by ultracentrifugation. Viral titers were measured by quantitative polymerase chain reaction (Rotor-Gene Q, QIAGEN).

Stereotaxic surgeries

Mice were anesthetized with intraperitoneal injection of pentobarbital (83 mg/kg of body weight). Ophthalmic ointment (liposic gel, BAUSCH and LOMB) was applied to the eyes of the mice to prevent dehydration. Virus was injected with glass capillary filled with water and 2 μl of mineral oil (Sigma-Aldrich, M5904-500ML) at the tip. The injection pipette was placed at the injection site for additional 10 min post-surgery for diffusion of virus.

For manipulation of $CGRP^{PBN}$ neurons, $Calca^{Cre}$ mice receives bilateral injection of virus (0.45 μl per side) using the following coordinate: PBN [anterior-psoterior (AP), −5.0 mm; medial-lateral (ML), ±1.4 mm; dorso-ventral (DV), −3.55 mm]. For optogenetic inhibition of $CGRP^{PBN}$ neurons, the optic fibers (Doric lenses, 200-μm core diameter, 0.37 numerical aperture (NA) for optogenetic manipulation) were implanted using the following coordinate: PBN (AP, −5.0 mm; ML, ±1.75 mm; DV, −3.1 mm). For fiber photometry of $CGRP^{PBN}$ neurons, the optic fiber [RWD Life Science Co., Ltd. (RWD), 400 μm core diameter, 0.5 NA] was implanted unilaterally on the right PBN. The mice underwent behavioral testing after a 2-week recovery period.

For unilateral retrograde tracing, $Calca^{Cre}$ mice received unilateral injection of helper virus (AAV-hsyn-DIO-TVA-HA-N2cG, 0.45 μl) into the right hemisphere of PBN [AP, −5.0 mm; ML, +1.4 mm; DV, −3.55 mm). Two weeks later, rabies virus (0.45 μl; EnvA-pseudotyped SADB19 Rb GFP) was injected into the same coordinate. Eight days later, mice were etuhanized for histological analysis. For bilateral retrograde tracing and c-Fos quantification, the injection surgeries were conducted on the bilateral PBN as above. Eight days later, behavioral tests were performed, and mice were euthanized for histological analysis.

To inhibit terminals of pIC-PBN pathways, C57BL/6J mice received bilateral injection of virus using the following coordinates: pIC (AP, −0.4 mm; ML, ±4.2 mm; DV, −4.0 mm; 0.4 μl per side). For optogenetic terminal inhibition, optic fiber (Doric Lenses, 200-μm core diameter, 0.37 NA) was implanted right above the PBN (AP, −5.0 mm; ML, ±1.75 mm; DV, −3.1 mm). Behavioral experiments were conducted 3 weeks after virus injection.

For fiber photometry of $CGRP^{PBN}$ neurons, AAV1-hsyn-DIO-GCaMP6m was unilaterally injected into the right PBN (AP, −5.0 mm; ML, +1.4 mm; DV, −3.55 mm), and optic fiber (RWD, 400-μm core diameter, 0.5 NA) was implanted on the PBN (AP, −5.0 mm; ML, +1.75 mm; DV, −3.1 mm). For fiber photometry of $CGRP^{PBN}$ neurons with hM4Di inhibition of $pIC^{\rightarrow PBN}$ neurons, we bilaterally injected AAV8-hsyn-fDIO-hM4Di-mCehrry into the pIC and AAVretro-Ef1α-FlpO into the PBN of $Calca^{Cre}$ mice. Ten days later, AAV1-hsyn-DIO-GCaMP6m was unilaterally injected into the right PBN (AP, −5.0 mm; ML, +1.4 mm; DV, −3.55 mm), and optic fiber (RWD, 400-μm core diameter, 0.5 NA) was implanted on the PBN (AP, −5.0 mm; ML, +1.75 mm; DV, −3.1 mm). After 2-week recovery period, the fiber photometry experiments were conducted.

For fiber photometry of $pIC^{\rightarrow CGRP\text{-}PBN}$ neurons, helper virus (0.45 μl; AAV-hS-DIO-TVA-HA-N2cG) was injected into the PBN (AP, −5.0 mm; ML, +1.4 mm; DV, −3.55 mm). Two weeks later, the rabies virus (EnvA pseudotyped N2c Rb-mCherry-FlpO, 0.45 μl) was injected into the same site of PBN, and the AAV8-Ef1α-fDIO-GCaMP6s was injected into the ipsilateral pIC (AP, −0.4 mm; ML, +4.2 mm; DV, −4.0 mm; 0.4 μl), respectively. Optic fiber (RWD, 400-μm core diameter, 0.5 NA) was implanted on the pIC (AP, −0.4 mm; ML, +4.2 mm; DV, −3.6 mm). After a 2-week recovery period, the fiber photometry experiments were conducted.

For ChR2 activation of pIC-$CGRP^{PBN}$ circuit, helper virus (AAV-hS-DIO-TVA-HA-N2cG, 0.45 μl) was injected into the bilateral PBN (AP, −5.0 mm; ML, ±1.4 mm; DV, −3.55 mm; 0.45 μl), and AAV8-Ef1α-fDIO-hChR2-EYFP was injected into the bilateral pIC (AP, −0.4 mm; ML, ±4.2 mm; DV, −3.6 mm; 0.4 μl). Two weeks later, the rabies virus (EnvA-pseudotyped N2c Rb-mCherry-FlpO; 0.45 μl) was injected into the same site of bilateral PBN, and optic fibers (Doric Lenses, 200-μm core diameter, 0.37 NA) were implanted on the PBN (AP, −5.0 mm; ML, ±1.75 mm; DV, −3.1 mm). After a 2-week recovery period, the ChR2 activation experiments were conducted.

For axon tracing of $PIC^{\rightarrow PBN}$ neurons, we injected AAVretro-Ef1α-FlpO into the unilateral PBN and AAVdj-hsyn-fDIO-mGFP-2A-Synaptophysin-mRuby into the ipsilateral side of pIC. After 3 weeks, the mice were euthanized for histological analysis.

Behavioral procedures

Looming visual stimuli and behavioral apparatus

The looming visual stimuli were generated using custom software in the LabVIEW (National Instruments) environment and displayed

on an overhead liquid crystal display monitor (38 cm by 22 cm, 60-Hz refresh rate, Intehill). The monitor was positioned 30 cm above the mice and presented a white background. For the looming visual stimuli, a dark disc expanded from 5° (2.6 cm) to 35° (18.9 cm) of visual angle over 300 ms, remained on the screen for 500 ms, and was repeated five times (4 s) during conditioning and 10 times (8 s) during the behavioral response test, respectively. For the flickering visual stimuli, a 35° (18.9 cm) dark disc appeared on the monitor for 0.8 s, disappeared for 0.8 s, and this sequence was repeated five times (8 s).

The behavioral arena was surrounded by white acrylic walls, with one of the four walls being transparent (35-cm long, 35-cm wide, 30-cm high). During the experiments, the mouse's behavior was recorded through the transparent wall using a video camera positioned diagonally over the arena. The video was captured at a frame rate of 30 frames per s (FPS) using LabVIEW software.

Innate behavioral responses to looming visual stimuli

All animals were handled for 3 days before behavioral tests. To assess innate defensive responses to looming visual stimuli, mice were moved to the behavioral arena from their home cages. After more than 2 min of baseline exploration period, mice were exposed to looming visual stimuli for 8 s (10 repetitions of an expanding dark disc). One minute after the exposure to the looming stimuli, animals were removed from the arena and returned to their home cages. To evaluate the habituation effect to the looming visual stimuli, the immediate response test was conducted for five consecutive days. In a single-day habituation test, mice were exposed to the visual stimuli 10 times, with a 2-min interval between stimuli. The baseline freezing level was measured for 120 s during the prestimulus period before the onset of looming visual stimuli, and the looming-evoked freezing level was measured for 8 s during the visual stimuli presentation period.

Open-field test

In the TetTox inhibition experiment, an open-field test was performed before visual threat conditioning to confirm that there were no differences in basal locomotion and anxiety levels between groups. Mice were placed in an open-field arena (45-cm long, 45-cm wide, 30-cm high) and allowed to freely explore for 15 min. Freezing levels, total distance traveled, and time spent in the center area of the arena were measured.

Visual threat conditioning and fear memory retrieval test

All animals were handled for 3 days before behavioral tests. The conditioning chamber was a white acrylic box with one transparent wall, measuring 35 cm in length, 35 cm in width, and 30 cm in height. The floor was covered with paper pads. After 5 min of baseline exploration, mice were exposed to a 20-s auditory tone (CS, 2.7 kHz, 80 dB) that was coterminated with 4-s looming visual stimuli (US, a dark disc expanding five times). After five CS-US pairings with a 2-min interval, mice were removed from the conditioning chamber. In the unpaired conditioning protocol, the same auditory tone was presented but with random intervals, ranging from 15 to 30 s after the looming visual stimuli. The baseline freezing level was measured for 120 s during the pre-CS period immediately before the tone onset. Freezing levels for the CS and CS + US periods were measured during the first 16 s and last 4 s of CS-US pairing, respectively.

One day after conditioning, an auditory fear memory test was conducted. The mice were placed in a test chamber with a shifted context: a semicircular arena, striped walls, and a white acrylic floor (35-cm long, 35-cm wide, 30-cm high). After more than 2 min of exploration, the conditioned tone was presented for 20 s. Freezing behavior was measured during the pre-CS period (120 s) and the CS period (20 s).

Contextual fear memory test was conducted the following day. Mice were re-exposed to the conditioning chamber for 5 min, and freezing behavior was measured during the first 2 min to assess contextual fear memory.

Foot-shock threat conditioning and fear memory retrieval test

All mice underwent 3 days of handling before behavioral testing. For foot-shock conditioning, mice explored a conditioning chamber equipped with a metal grid floor (Med Associates, 25-cm long, 30-cm wide, 20-cm high) for 5 min. Subsequently, they were exposed to a 20-s auditory tone (CS, 2.7 kHz, 80 dB) that was coterminated with a 2-s foot-shock stimulus (US, 0.5 mA). The CS-US pairing was repeated five times with a 2-min interval. The average of baseline movement was measured for 120 s during the pre-CS period immediately before the onset of foot-shock. Movement for the CS and CS + US periods was measured for the first 16 s and the last 4 s during CS-US pairing, respectively.

One day after foot-shock conditioning, an auditory fear memory test was conducted. Mice were placed in a test chamber with a shifted context: a semicircular arena, striped walls, and a white acrylic floor (Med Associates, 25-cm long, 30-cm wide, 20-cm high). After more than 2 min of exploration, the conditioned tone was presented for 20 s. Freezing behavior was measured during the pre-CS period (120 s) and the CS period (20 s).

Optogenetic inhibition behavior experiments

All mice underwent three days of handling before behavioral testing. To habituate them to the optical manipulation procedure, they were tethered to fiber-optic patch cords for 5 min/day over three consecutive days.

For optogenetic eNpHR3.0 inhibition during conditioning, optical inhibition (561 nm, continuous; 3 to 5 mW at the fiber tip for soma inhibition, 10 mW for terminal inhibition) began 2 s before the first US exposure and continued until the end of the experiment. For optogenetic inhibition during the tone retrieval test, optical inhibition was applied throughout the 20-s presentation of the tone-CS and terminated immediately afterward.

For optogenetic inhibition during the US exposure experiment, inhibition was initiated 2 s before US onset and terminated 2 s after US offset, lasting a total of 8 s per trial. For optogenetic inhibition during the ITI, inhibition started immediately after US exposure and ended just before the next US exposure, lasting 2 min per trial.

Optogenetic stimulation behavior experiments

All mice underwent 3 days of handling before behavioral testing. In addition, mice were tethered to fiber-optic patch cords for 5 min per day over three consecutive days to habituate them to the optic manipulation procedure.

To assess the anxiogenic effects of stimulating the pIC-CGRP^{PBN} pathway, we conducted the RTPA test, open-field test, and EPM test sequentially. In the RTPA test, the three-chamber arena was used (25-cm long, 75-cm wide, and 25-cm high; two side chambers with 30-cm wide each, and a middle chamber with 15-cm wide). One of the side chambers had a striped wall and metal grid floor, while the other had a checkered wall and punched metal floor. During the test, mice explored the arena for total 30 min. The first 10-min was used to determine a baseline chamber preference between the two side chambers. The chamber with more preference was selected for pairing with photostimulation. During the last 10 min, optical

stimulation (473 nm, 20 Hz, 10 ms pulse, 10 mW at the fiber tip) was applied only when mice entered the selected side chamber. To assess the avoidance behavior induced by photostimulation, the time spent in each side chamber during the pretest (the first 10 min) and test period (the last 10 min) was compared. The preference ratio was calculated by dividing the time spent in the photostimulation-paired chamber during the test by the time spent in the same chamber during the pretest. The difference score was calculated by subtracting time spent in each chamber (left, middle, and right) during the pretest from during the test. One mouse that spent more than 70% of the time in one of the two side chambers during the pretest period was excluded from the analysis.

In the open-field test, to evaluate the effect of optical stimulation on immediate freezing and anxiogenic behaviors, mice were allowed to explore an open-field arena (45 cm by 45 cm by 30 cm). After 2-min exploration, the mice were exposed to a 30 s-photostimulation (473 nm, 20 Hz, 10-ms pulse, 10 mW at the fiber tip) session five times with a 60-s interval. Measures included freezing behavior, time spent in the center zone, the number of center crossings, and total distance traveled. The center zone was defined as a 20-cm square area in the center of the arena.

In the EPM test, the arena was a cross-shaped acrylic structure with 65 cm in length and 5 cm in width. Two closed arms were enclosed by 16-cm high white acrylic walls, while the open arms have 0.5-cm high transparent acrylic walls. Mice were allowed to explore the EPM arena freely for 10 min, during which they were exposed to photostimulation with a 2-s on and 2-s off cycle. To evaluate anxiety behavior, the time spent in the open and closed arms, the number of entries into each arm, and the total distance traveled during the 10-min test were measured.

For optic conditioning, mice were allowed to explore a conditioning chamber equipped with a metal grid floor (Med Associates, 25-cm long, 30-cm wide, 20-cm high) for 5 min. Subsequently, they were exposed to a 30-s auditory tone (CS, 2.7 kHz, 80 dB) that was coterminated with a 10-s photostimulation (US, 473 nm, 20 Hz, 10-ms pulse, 10 mW at the fiber tip). The CS-US pairing was repeated five times with a 2-min interval. One day after conditioning, mice were tested for auditory fear memory. Mice were placed in a test chamber with a shifted context: a semicircular arena, striped walls, and a white acrylic (Med Associates, 25-cm long, 30-cm wide, 20-cm high). After more than 2 min of exploration, the conditioned tone was presented for 30 s. Freezing behavior was measured during the pre-CS period (120 s) and the CS period (30 s).

c-Fos imaging behavior experiments

To assess c-Fos levels in the projection neurons upstream to $CGRP^{PBN}$ neurons in response to looming visual stimuli, behavioral experiments were conducted 8 days after rabies virus injection. Mice were allowed to freely explore the test arena for 5 min before being exposed to visual stimuli (either looming visual stimuli for 8 s with 10 expansions or flickering visual stimuli for 8 s with five flickers) twice at a 120-s interval. The mice were then returned to their home cages and euthanized 90 min after the first stimulus exposure.

Fiber photometry

For fiber photometry, a 400-μm diameter, 0.48-NA patch cord was used to collect fluorescence emission. A real-time signal processor [Tucker-Davis Technologies (TDT), RZ5P] controlled the 470 nm (Thorlabs, M470F3) and 405 nm (Doric, LEDC1-405_FC) light-emitting diodes (LEDs) and simultaneously recorded GCaMP (GFP-based Calcium Indicator) fluorescence emission. The 470-nm LED was sinusoidally modulated at 331 Hz to excite GCaMP, while the 405-nm LED was modulated at 531 Hz to monitor the isosbestic signal. The 470- and 405-nm light passed through a bandpass filter in a mini cube (Doric, FMC5) and into the optic fiber connected to the brain of mice. The emitted GCaMP6m signal was detected by a photoreceiver (New Focus, Model 2151) and digitized at 1017.3 Hz by the RZ5P processor. Fluorescence measurements (<6 Hz) were extracted from Synapse software (TDT), and further data processing was performed in MATLAB. $\Delta F/F$ was calculated by applying a least-squares linear fit to the 405 nm signal, aligning it with the 470-nm signal (fitted 405 nm), and then computing $\Delta F/F$ as (470 nm − fitted 405 nm)/fitted 405 nm.

Behavioral experiments were recorded at 30 FPS, with stimulus delivery and video capture controlled by a custom LabView program. To synchronize photometry recording with behavioral events (e.g., tone, visual stimuli, and shock), digital signals generated by LabView were recorded by the RZ5P processor.

To record calcium activity of $CGRP^{PBN}$ neurons in response to flickering and looming visual stimuli, mice were placed in the looming test chamber and allowed to explore freely for 5 min before stimulus presentation. First, they were exposed to flickering stimuli, followed by looming stimuli after a 5-min interval.

To examine calcium activity of $CGRP^{PBN}$ neurons while chemogenetically inhibiting $pIC^{\rightarrow PBN}$ neurons, DREADD agonist 21 dihydrochloride (C21; Tocris, #6422; working solution of 0.2 mg/ml and stock of 10 mg/ml) was administered via intraperitoneal injection at a dose of 1 mg/kg. One hour after C21 injection, mice were placed in the looming test chamber, where they explored for 5 min before being exposed to two looming stimuli (8 s) at a 120-s interval. After a 10-min rest, mice were transferred to a foot-shock chamber, where they explored for 5 min before receiving two foot shocks (2 s, 0.5 mA) at a 120-s interval. To compare $\Delta F/F$ across animals during stimulus exposure, $\Delta F/F$ was normalized to a z score, calculated as [($\Delta F/F$ − mean of $\Delta F/F_{baseline}$)/SD of $\Delta F/F_{baseline}$], where the baseline mean and standard deviation were computed from −5 to 0 s before stimulus onset.

To record the calcium response of $pIC^{\rightarrow CGRP\text{-}PBN}$ neurons to visual or foot-shock stimuli, mice were first placed in the looming test chamber, where they explored freely for 5 min before being exposed to looming visual stimuli (or flickering stimuli). The looming (or flickering) stimuli presented twice at a 120-s interval. After a 10-min rest period, mice were transferred to the foot-shock chamber, where they explored freely for 5 min before receiving two foot shocks (2 s, 0.5 mA) at a 120-s interval. As $pIC^{\rightarrow CGRP\text{-}PBN}$ neurons exhibited sustained calcium activity in response to both looming and shock stimuli, only the first 60 s of recording data from stimulus onset were included in the analysis. To minimize the effect of natural fluctuations in pIC neuronal activity, the baseline for z- scoring was computed from the 60-s period preceding stimulus onset (−60 to 0 s). To determine the peak and the time to half of the peak in calcium activity, z-scored calcium activity was filtered using a 1-Hz low-pass filter. The maximum peak was identified within the 0- to 100-s time window following stimulus onset. After determining the peak time, the time point at which calcium activity declined to half of the peak value was identified. Because $pIC^{\rightarrow CGRP\text{-}PBN}$ neurons exhibited persistent but distinct response dynamics to looming and shock stimuli, we analyzed their responses based on the half-peak time window: 0 to 60 s for looming and 0 to 20 s for shock.

Analysis of behaviors

Freezing was defined as a state in which the mouse remained completely immobile except for respiratory movements. Running was defined as when the centroid of the mouse body moved at a velocity of 40 cm/s or greater. All other behaviors were classified as no response. The centroid of the subjects was analyzed to determine position, calculate velocity, and track movement trajectories. Centroid was detected by using custom MATLAB scripts. Brightness thresholds were manually set to differentiate the pixels corresponding to the mouse. Perspective distortion from the camera lens was corrected using the tform function in MATLAB. Velocity was calculated from the centroid data and smoothed using a mean filter.

Histology

For histological verification of virus expression and optic fiber placement, brain sections were prepared from the euthanized mice after the end of behavioral experiments. Mice were anesthetized with 2.5% avertin by intraperitoneal injection, and they were perfused transcardially with PBS and then fixed with ice-cold 4% paraformaldehyde (PFA). After perfusion, brain samples were stored in 4% PFA overnight for post-fixation and sliced in a 40-μm thickness afterward by using a vibratome (VT-1200S, Leica Microsystems).

For a retrograde tracing and c-Fos staining, mice underwent behavioral experiments 8 days after the rabies virus injection and were euthanized 90 min after exposure to visual stimuli. Mice were anesthetized with pentobarbital (83 mg/kg of body weight) by intraperitoneal injection, perfused transcardially with phosphate-buffered saline (PBS), and then fixed with ice-cold 4% PFA. After perfusion, brain samples were stored in 4% PFA overnight for post-fixation. Fixed brain samples were dehydrated in a series of 10, 20, and 30% filtered sucrose solutions (#S0389, Sigma-Aldrich) until they sank to the bottom of vials. Dehydrated brain samples were attached on a specimen disc with OCT compounds (#4583, Scigen) at −20°C. Brains were coronally sliced in a 40-μm thickness by using a Cryostat (Leica CM1850, Leica Biosystems).

Brain sections were mounted on a gelatin-coated slide glass with a VECTASHIELD antifade mounting media (h-2000, Vector Laboratories). Images were taken for histological verification by using a confocal microscope (LSM880, Carl Zeiss) or slide scanner (Zeiss Axio Scan.Z1, Carl Zeiss). By reference to the Mouse Brain Atlas, the mice who showed off-target viral expression in surrounding areas or displacement of ferrules were excluded.

Immunohistochemistry

For immunostaining, brain sections were washed three times with PBS and incubated in blocking solution (2% goat serum, 0.1% bovine serum albumin, and 0.2% Triton X-100 in PBS) for 1 hour on an orbital shaker (126 rpm). Brain sections were incubated in a primary antibody solution on the orbital shaker (126 rpm) overnight at room temperature (RT). After brain sections were washed four times with PBS, sections were then incubated in a secondary antibody solution on the shaker (126 rpm) for 2 hours. Subsequently, the brain sections underwent four additional washes with PBS. Immunostained brain sections were transferred to gelatin-coated slides using a brush. Sections were stained with 4′,6-diamidino-2-phenylindole (DAPI) (0.5 μg/ml in PBS; #D9542, Sigma-Aldrich) for 20 min at RT. The slides were rapidly immersed in a distilled water and allowed to air-dry completely in a light-protected environment. Coverslip was mounted with a VECTASHIELD antifade mounting media (h-2000, Vector Laboratories).

The dTomato fluorescence signals in neurons injected with AAV-TetTox-P2A-nls-dTomato virus were amplified with mouse anti-DsRed primary antibody (1:500; #SC-390909, Santa Cruz Biotechnology) and Alexa Fluor 594–conjugated goat anti-mouse secondary antibody (1:2000; #A-11005, Molecular Probes). The EYFP fluorescence signals in neurons injected with AAV-CaMKIIα-eNpHR3.0-EYFP virus were amplified with rabbit anti-GFP primary antibody (1:5000; #ab290, Abcam) and Alexa Fluor 488–conjugated goat anti-rabbit secondary antibody (1:2000; #A-11008, Molecular Probes). The antibodies used for hemagglutinin (HA) staining were rabbit anti-HA (1:1000; #3724, Cell signaling) and Alexa Fluor 647–conjugated goat anti-rabbit (1:2000; #A-21244, Molecular Probes). The antibodies used for c-Fos staining were rabbit anti-cFos (1:2000; rabbit anti-cFos; #226008, Synaptic systems) and Alexa Fluor 594–conjugated goat anti-rabbit (1:2000; Alexa Fluor 594–conjugated goat anti-rabbit; #A-11037, Molecular Probes). In axon tracing experiment, mGFP and synaptophysin-mRuby were amplified with rabbit anti-GFP primary antibody (1:5000; #ab290, Abcam), mouse anti–red fluorescent protein primary antibody (1:2000; # 200-301-379, Rockland), Alexa Fluor 488–conjugated goat anti-rabbit secondary antibody (1:2000; #A-11008, Molecular Probes), and Alexa Fluor 594–conjugated goat anti-mouse (1:2000; #A-11005, Molecular Probes).

For anterograde tracing of the $pIC^{\rightarrow PBN}$ neurons, Sudan black B (SBB) staining was performed. After DAPI staining, the samples were stained with 0.1% SBB for 20 min at RT. The sections were briefly rinsed with 70% ethanol for 30 s, followed by a 5-min rinse in PBS. The 0.3% SBB stock solution (in 70% ethanol) was stirred overnight in the dark and filtered using a 0.22-μm filter. The 0.1% SBB working solution was freshly prepared before use.

Cell counting analysis

To map the location of retrogradely labeled GFP^+ cells throughout the whole brain, coronal brain tissues were collected along AP axis [from anterior part (AP, +1.8 mm) to posterior part (AP, −5.5 mm)] in a 120-μm distance. For the brain-wide tracing, images of all brain sections were captured using a Slide scanner (Zeiss Axio Scan.Z1, Carl Zeiss). The number of $DAPI^+$ and GFP^+ cells in the brain sections were then counted by using the AMaSiNe automatic cell counting software (*83*) by registering brain images to the Allen Brain Atlas Common Coordinate Framework (CCFv3) (*84*).

To assess the overlap between $c\text{-}Fos^+$ and GFP^+ cells, we conducted c-Fos immunostaining, and optical sections (2 μm per section) were obtained using confocal microscopy with Z-stack analysis. $DAPI^+$, GFP^+, and $c\text{-}Fos^+$ cells were detected using the AMaSiNe cell counting algorithm (*83*). Regions of interest (ROI) were then defined in each target area, and the overlap between $c\text{-}Fos^+$ and GFP^+ cells was manually counted in a blinded manner. The AP ranges for c-Fos quantification in each target brain area are: pIC (AP, −0.2 to −0.6 mm), CeA (AP, −1.2 to −1.6 mm), PAG (AP, −3.5 to −3.9 mm), and SC (AP, −3.5 to −3.9 mm). To compare $CGRP^{PBN}$-projecting neurons in the aIC and pIC, we counted GFP^+ cells in the aIC (AP, +1.0 to 0 mm) and pIC (AP, 0 to −1.0 mm).

Statistical analysis

GraphPad Prism 10.0.2 was used for graph generation and statistical analyses. The Shapiro-Wilk test was used to assess data normality. For datasets with a small sample size ($N < 7$), the Kolmogorov-Smirnov test was conducted, and data distribution was additionally evaluated using Quantile-Quantile plots. Paired or unpaired Student's *t* tests

were performed to compare normally distributed datasets of experimental and control groups depending on experimental design. Wilcoxon matched pairs signed-rank test or Mann-Whitney test were performed to compare non-normally distributed datasets of experimental and control groups. One-way analysis of variance (ANOVA) and repeated-measures two-way ANOVA, followed by Sidak's post hoc test, were used to analyze behavioral tasks depending on the experimental design. Differences were considered statistically significant if the *P* value was below 0.05. Error bars represent the SEM. More details are provided in the table S1.

Supplementary Materials

The PDF file includes:
Figs. S1 to S6
Legend for table S1
Legend for data file S1

Other Supplementary Material for this manuscript includes the following:
Table S1
Data file S1

REFERENCES AND NOTES

1. T. Beckers, D. Hermans, I. Lange, L. Luyten, S. Scheveneels, B. Vervliet, Understanding clinical fear and anxiety through the lens of human fear conditioning. *Nat. Rev. Psychol.* **2**, 233–245 (2023).
2. J. E. LeDoux, Emotion, memory and the brain. *Sci. Am.* **270**, 50–57 (1994).
3. M. S. Fanselow, What is conditioned fear? *Trends Neurosci.* **7**, 460–462 (1984).
4. J. E. LeDoux, Emotion circuits in the brain. *Annu. Rev. Neurosci.* **23**, 155–184 (2000).
5. J. F. Medina, J. Christopher Repa, M. D. Mauk, J. E. LeDoux, Parallels between cerebellum- and amygdala-dependent conditioning. *Nat. Rev. Neurosci.* **3**, 122–131 (2002).
6. J. P. Johansen, C. K. Cain, L. E. Ostroff, J. E. LeDoux, Molecular mechanisms of fear learning and memory. *Cell* **147**, 509–524 (2011).
7. C. T. Gross, N. S. Canteras, The many paths to fear. *Nat. Rev. Neurosci.* **13**, 651–658 (2012).
8. P. Tovote, J. P. Fadok, A. Lüthi, Neuronal circuits for fear and anxiety. *Nat. Rev. Neurosci.* **16**, 317–331 (2015).
9. L. K. Takahashi, M. M. Chan, M. L. Pilar, Predator odor fear conditioning: Current perspectives and new directions. *Neurosci. Biobehav. Rev.* **32**, 1218–1227 (2008).
10. D. C. Blanchard, G. Griebel, R. J. Blanchard, Conditioning and residual emotionality effects of predator stimuli: Some reflections on stress and emotion. *Prog. Neuropsychopharmacol. Biol. Psychiatry* **27**, 1177–1185 (2003).
11. M. Yilmaz, M. Meister, Rapid innate defensive responses of mice to looming visual stimuli. *Curr. Biol.* **23**, 2011–2015 (2013).
12. L. K. Takahashi, D. T. Hubbard, I. Lee, Y. Dar, S. M. Sipes, Predator odor-induced conditioned fear involves the basolateral and medial amygdala. *Behav. Neurosci.* **121**, 100–110 (2007).
13. N. S. Pentkowski, D. C. Blanchard, C. Lever, Y. Litvin, R. J. Blanchard, Effects of lesions to the dorsal and ventral hippocampus on defensive behaviors in rats. *Eur. J. Neurosci.* **23**, 2185–2196 (2006).
14. D. C. Blanchard, N. S. Canteras, C. M. Markham, N. S. Pentkowski, R. J. Blanchard, Lesions of structures showing FOS expression to cat presentation: Effects on responsivity to a Cat, Cat odor, and nonpredator threat. *Neurosci. Biobehav. Rev.* **29**, 1243–1253 (2005).
15. M. Rodríguez, F. Ceric, P. Murgas, B. Harland, F. Torrealba, M. Contreras, Interoceptive insular cortex mediates both innate fear and contextual threat conditioning to predator odor. *Front. Behav. Neurosci.* **13**, 283 (2020).
16. K. J. Wallace, J. B. Rosen, Predator odor as an unconditioned fear stimulus in rats: Elicitation of freezing by trimethylthiazoline, a component of fox feces. *Behav. Neurosci.* **114**, 912–922 (2000).
17. R. J. Blanchard, M. Yang, C. I. Li, A. Gervacio, D. C. Blanchard, Cue and context conditioning of defensive behaviors to cat odor stimuli. *Neurosci. Biobehav. Rev.* **25**, 587–595 (2001).
18. L. K. Takahashi, Olfactory systems and neural circuits that modulate predator odor fear. *Front. Behav. Neurosci.* **8**, 72 (2014).
19. A. Cruz, M. Heinemans, C. Marquez, M. A. Moita, Freezing displayed by others is a learned cue of danger resulting from co-experiencing own freezing and shock. *Curr. Biol.* **30**, 1128–1135.e6 (2020).
20. D. C. Blanchard, C. Markham, M. Yang, D. Hubbard, E. Madarang, R. J. Blanchard, Failure to produce conditioning with low-dose trimethylthiazoline or cat feces as unconditioned stimuli. *Behav. Neurosci.* **117**, 360–368 (2003).
21. G. De Franceschi, T. Vivattanasarn, A. B. Saleem, S. G. Solomon, Vision guides selection of freeze or flight defense strategies in mice. *Curr. Biol.* **26**, 2150–2154 (2016).
22. G. Baranauskas, N. Svirskiene, G. Svirskis, 20Hz membrane potential oscillations are driven by synaptic inputs in collision-detecting neurons in the frog optic tectum. *Neurosci. Lett.* **528**, 196–200 (2012).
23. T. W. Dunn, C. Gebhardt, E. A. Naumann, C. Riegler, M. B. Ahrens, F. Engert, F. Del Bene, Neural circuits underlying visually evoked escapes in larval zebrafish. *Neuron* **89**, 613–628 (2016).
24. K. Bhattacharyya, D. L. McLean, M. A. MacIver, Visual threat assessment and reticulospinal encoding of calibrated responses in larval zebrafish. *Curr. Biol.* **27**, 2751–2762.e6 (2017).
25. W. Schiff, J. A. Caviness, J. J. Gibson, Persistent fear responses in rhesus monkeys to the optical stimulus of "looming". *Science* **136**, 982–983 (1962).
26. J. Náñez Sr., Perception of impending collision in 3-to 6-week-old human infants. *Infant Behav. Dev.* **11**, 447–463 (1988).
27. W. Schiff, Perception of impending collision: A study of visually directed avoidant behavior. *Psychol. Monogr.* **79**, 1–26 (1965).
28. S. Maren, Neurobiology of Pavlovian fear conditioning. *Annu. Rev. Neurosci.* **24**, 897–931 (2001).
29. B. A. Pellman, J. J. Kim, What can ethobehavioral studies tell us about the brain's fear system? *Trends Neurosci.* **39**, 420–431 (2016).
30. J. E. LeDoux, Coming to terms with fear. *Proc. Natl. Acad. Sci. U.S.A.* **111**, 2871–2878 (2014).
31. H. C. Pape, D. Pare, Plastic synaptic networks of the amygdala for the acquisition, expression, and extinction of conditioned fear. *Physiol. Rev.* **90**, 419–463 (2010).
32. R. P. Vertes, S. B. Linley, W. B. Hoover, Limbic circuitry of the midline thalamus. *Neurosci. Biobehav. Rev.* **54**, 89–107 (2015).
33. L. G. Reijmers, B. L. Perkins, N. Matsuo, M. Mayford, Localization of a stable neural correlate of associative memory. *Science* **317**, 1230–1233 (2007).
34. P. W. Frankland, B. Bontempi, L. E. Talton, L. Kaczmarek, A. J. Silva, The involvement of the anterior cingulate cortex in remote contextual fear memory. *Science* **304**, 881–883 (2004).
35. J. A. Boatman, J. J. Kim, A thalamo-cortico-amygdala pathway mediates auditory fear conditioning in the intact brain. *Eur. J. Neurosci.* **24**, 894–900 (2006).
36. J. P. Johansen, H. L. Fields, Glutamatergic activation of anterior cingulate cortex produces an aversive teaching signal. *Nat. Neurosci.* **7**, 398–403 (2004).
37. S. Han, M. T. Soleiman, M. E. Soden, L. S. Zweifel, R. D. Palmiter, Elucidating an affective pain circuit that creates a threat memory. *Cell* **162**, 363–374 (2015).
38. C. A. Campos, A. J. Bowen, C. W. Roman, R. D. Palmiter, Encoding of danger by parabrachial CGRP neurons. *Nature* **555**, 617–622 (2018).
39. S. J. Kang, S. Liu, M. Ye, D. I. Kim, G. M. Pao, B. A. Copits, B. Z. Roberts, K. F. Lee, M. R. Bruchas, S. Han, A central alarm system that gates multi-sensory innate threat cues to the amygdala. *Cell Rep.* **40**, 111222 (2022).
40. K. E. Krout, A. S. Jansen, A. D. Loewy, Periaqueductal gray matter projection to the parabrachial nucleus in rat. *J. Comp. Neurol.* **401**, 437–454 (1998).
41. A. J. Todd, Neuronal circuitry for pain processing in the dorsal horn. *Nat. Rev. Neurosci.* **11**, 823–836 (2010).
42. S. P. Hunt, P. W. Mantyh, The molecular dynamics of pain control. *Nat. Rev. Neurosci.* **2**, 83–91 (2001).
43. C. Shang, Z. Chen, A. Liu, Y. Li, J. Zhang, B. Qu, F. Yan, Y. Zhang, W. Liu, Z. Liu, X. Guo, D. Li, Y. Wang, P. Cao, Divergent midbrain circuits orchestrate escape and freezing responses to looming stimuli in mice. *Nat. Commun.* **9**, 1232 (2018).
44. P. Wei, N. Liu, Z. Zhang, X. Liu, Y. Tang, X. He, B. Wu, Z. Zhou, Y. Liu, J. Li, Y. Zhang, X. Zhou, L. Xu, L. Chen, G. Bi, X. Hu, F. Xu, L. Wang, Processing of visually evoked innate fear by a non-canonical thalamic pathway. *Nat. Commun.* **6**, 6756 (2015).
45. T. L. Krukoff, K. H. Harris, J. H. Jhamandas, Efferent projections from the parabrachial nucleus demonstrated with the anterograde tracer Phaseolus vulgaris leucoagglutinin. *Brain Res. Bull.* **30**, 163–172 (1993).
46. K. Tokita, T. Inoue, J. D. Boughter Jr., Afferent connections of the parabrachial nucleus in C57BL/6J mice. *Neuroscience* **161**, 475–488 (2009).
47. P. Rainville, B. Carrier, R. K. Hofbauer, M. C. Bushnell, G. H. Duncan, Dissociation of sensory and affective dimensions of pain using hypnotic modulation. *Pain* **82**, 159–171 (1999).
48. T. Singer, B. Seymour, J. O'Doherty, H. Kaube, R. J. Dolan, C. D. Frith, Empathy for pain involves the affective but not sensory components of pain. *Science* **303**, 1157–1162 (2004).
49. D. D. Price, Psychological and neural mechanisms of the affective dimension of pain. *Science* **288**, 1769–1772 (2000).
50. A. C. de C. Williams, K. D. Craig, Updating the definition of pain. *Pain* **157**, 2420–2423 (2016).
51. R. D. Palmiter, The parabrachial nucleus: CGRP neurons function as a general alarm. *Trends Neurosci.* **41**, 280–293 (2018).
52. M. E. Carter, M. E. Soden, L. S. Zweifel, R. D. Palmiter, Genetic identification of a neural circuit that suppresses appetite. *Nature* **503**, 111–114 (2013).
53. J. C. Kim, M. N. Cook, M. R. Carey, C. Shen, W. G. Regehr, S. M. Dymecki, Linking genetically defined neurons to behavior through a broadly applicable silencing allele. *Neuron* **63**, 305–315 (2009).

54. D. C. Castro, K. C. Berridge, Opioid and orexin hedonic hotspots in rat orbitofrontal cortex and insula. *Proc. Natl. Acad. Sci. U.S.A.* **114**, E9125–E9134 (2017).
55. Y. Peng, S. Gillis-Smith, H. Jin, D. Tränkner, N. J. P. Ryba, C. S. Zuker, Sweet and bitter taste in the brain of awake behaving animals. *Nature* **527**, 512–515 (2015).
56. D. A. Gehrlach, N. Dolensek, A. S. Klein, R. R. Chowdhury, A. Matthys, M. Junghänel, T. N. Gaitanos, A. Podgornik, T. D. Black, N. R. Vaka, K.-K. Conzelmann, N. Gogolla, Aversive state processing in the posterior insular cortex. *Nat. Neurosci.* **22**, 1424–1437 (2019).
57. M. P. Paulus, M. B. Stein, An insular view of anxiety. *Biol. Psychiatry* **60**, 383–387 (2006).
58. H. Gündel, M. F. O'Connor, L. Littrell, C. Fort, R. D. Lane, Functional neuroanatomy of grief: An FMRI study. *Am. J. Psychiatry* **160**, 1946–1953 (2003).
59. N. I. Eisenberger, M. D. Lieberman, K. D. Williams, Does rejection hurt? An fMRI study of social exclusion. *Science* **302**, 290–292 (2003).
60. N. Grahek, *Feeling pain and being in pain* (MIT Press, 2011).
61. A. S. Klein, N. Dolensek, C. Weiand, N. Gogolla, Fear balance is maintained by bodily feedback to the insular cortex in mice. *Science* **374**, 1010–1015 (2021).
62. J. B. Nitschke, I. Sarinopoulos, K. L. Mackiewicz, H. S. Schaefer, R. J. Davidson, Functional neuroanatomy of aversion and its anticipation. *Neuroimage* **29**, 106–116 (2006).
63. T. Klucken, S. Kagerer, J. Schweckendiek, K. Tabbert, D. Vaitl, R. Stark, Neural, electrodermal and behavioral response patterns in contingency aware and unaware subjects during a picture–picture conditioning paradigm. *Neuroscience* **158**, 721–731 (2009).
64. Y. Livneh, A. U. Sugden, J. C. Madara, R. A. Essner, V. I. Flores, L. A. Sugden, J. M. Resch, B. B. Lowell, M. L. Andermann, Estimation of current and future physiological states in insular cortex. *Neuron* **105**, 1094–1111.e10 (2020).
65. Y. Livneh, M. L. Andermann, Cellular activity in insular cortex across seconds to hours: Sensations and predictions of bodily states. *Neuron* **109**, 3576–3593 (2021).
66. X. Chen, H. Choo, X. P. Huang, X. Yang, O. Stone, B. L. Roth, J. Jin, The first structure-activity relationship studies for designer receptors exclusively activated by designer drugs. *ACS Chem. Neurosci.* **6**, 476–484 (2015).
67. H. Li, M. A. Penzo, H. Taniguchi, C. D. Kopec, Z. J. Huang, B. Li, Experience-dependent modification of a central amygdala fear circuit. *Nat. Neurosci.* **16**, 332–339 (2013).
68. A. Adhikari, T. N. Lerner, J. Finkelstein, S. Pak, J. H. Jennings, T. J. Davidson, E. Ferenczi, L. A. Gunaydin, J. J. Mirzabekov, L. Ye, S. Y. Kim, A. Lei, K. Deisseroth, Basomedial amygdala mediates top-down control of anxiety and fear. *Nature* **527**, 179–185 (2015).
69. T. Nagashima, S. Tohyama, K. Mikami, M. Nagase, M. Morishima, A. Kasai, H. Hashimoto, A. M. Watabe, Parabrachial-to-parasubthalamic nucleus pathway mediates fear-induced suppression of feeding in male mice. *Nat. Commun.* **13**, 7913 (2022).
70. J. P. Johansen, J. W. Tarpley, J. E. Ledoux, H. T. Blair, Neural substrates for expectation-modulated fear learning in the amygdala and periaqueductal gray. *Nat. Neurosci.* **13**, 979–986 (2010).
71. C. Shang, Z. Liu, Z. Chen, Y. Shi, Q. Wang, S. Liu, D. Li, P. Cao, A parvalbumin-positive excitatory visual pathway to trigger fear responses in mice. *Science* **348**, 1472–1477 (2015).
72. A. J. Bowen, J. Y. Chen, Y. W. Huang, N. A. Baertsch, S. Park, R. D. Palmiter, Dissociable control of unconditioned responses and associative fear learning by parabrachial CGRP neurons. *eLife* **9**, e59799 (2020).
73. B. Hsueh, R. Chen, Y. Jo, D. Tang, M. Raffiee, Y. S. Kim, M. Inoue, S. Randles, C. Ramakrishnan, S. Patel, D. K. Kim, T. X. Liu, S. H. Kim, L. Tan, L. Mortazavi, A. Cordero, J. Shi, M. Zhao, T. T. Ho, A. Crow, A.-C. W. Yoo, C. Raja, K. Evans, D. Bernstein, M. Zeineh, M. Goubran, K. Deisseroth, Cardiogenic control of affective behavioural state. *Nature* **615**, 292–299 (2023).
74. A. Kennedy, P. S. Kunwar, L.-Y. Li, S. Stagkourakis, D. A. Wagenaar, D. J. Anderson, Stimulus-specific hypothalamic encoding of a persistent defensive state. *Nature* **586**, 730–734 (2020).
75. Y. N. Jan, L. Y. Jan, S. W. Kuffler, A peptide as a possible transmitter in sympathetic ganglia of the frog. *Proc. Natl. Acad. Sci. U.S.A.* **76**, 1501–1505 (1979).
76. D. A. Evans, A. V. Stempel, R. Vale, S. Ruehle, Y. Lefler, T. Branco, A synaptic threshold mechanism for computing escape decisions. *Nature* **558**, 590–594 (2018).
77. Z. Zhou, X. Liu, S. Chen, Z. Zhang, Y. Liu, Q. Montardy, Y. Tang, P. Wei, N. Liu, L. Li, R. Song, J. Lai, X. He, C. Chen, G. Bi, G. Feng, F. Xu, L. Wang, A VTA GABAergic neural circuit mediates visually evoked innate defensive responses. *Neuron* **103**, 473–488.e6 (2019).
78. P. R. Zambetti, B. P. Schuessler, B. E. Lecamp, A. Shin, E. J. Kim, J. J. Kim, Ecological analysis of Pavlovian fear conditioning in rats. *Commun. Biol.* **5**, 830 (2022).
79. R. A. Essner, A. G. Smith, A. A. Jamnik, A. R. Ryba, Z. D. Trutner, M. E. Carter, AgRP neurons can increase food intake during conditions of appetite suppression and inhibit anorexigenic parabrachial neurons. *J. Neurosci.* **37**, 8678–8687 (2017).
80. A. L. Alhadeff, Z. Su, E. Hernandez, M. L. Klima, S. Z. Phillips, R. A. Holland, C. Guo, A. W. Hantman, B. C. De Jonghe, J. N. Betley, A neural circuit for the suppression of pain by a competing need state. *Cell* **173**, 140–152.e15 (2018).
81. T. J. Roelofs, S. Menting-Henry, L. M. Gol, A. M. Speel, V. H. Wielenga, K. M. Garner, M. C. M. Luijendijk, A. A. Hennrich, K. K. Conzelmann, R. A. Adan, Optimization of whole-brain rabies virus tracing technology for small cell populations. *Sci. Rep.* **11**, 10400 (2021).
82. J. T. Kwon, R. Nakajima, H. S. Kim, Y. Jeong, G. J. Augustine, J. H. Han, Optogenetic activation of presynaptic inputs in lateral amygdala forms associative fear memory. *Learn. Mem.* **21**, 627–633 (2014).
83. J. H. Song, W. Choi, Y. H. Song, J. H. Kim, D. Jeong, S. H. Lee, S. B. Paik, Precise mapping of single neurons by calibrated 3D reconstruction of brain slices reveals topographic projection in mouse visual cortex. *Cell Rep.* **31**, 107682 (2020).
84. Q. Wang, S. L. Ding, Y. Li, J. Royall, D. Feng, P. Lesnar, N. Graddis, M. Naeemi, B. Facer, A. Ho, T. Dolbeare, B. Blanchard, N. Dee, W. Wakeman, K. E. Hirokawa, A. Szafer, S. M. Sunkin, S. W. Oh, A. Bernard, J. W. Phillips, M. Hawrylycz, C. Koch, H. Zeng, J. A. Harris, L. Ng, The Allen mouse brain common coordinate framework: A 3D reference atlas. *Cell* **181**, 936–953.e20 (2020).

Acknowledgments: We thank all members of the Memory Biology laboratory for helpful comments, discussions, and constructive suggestions. We thank the KAIST Bio-Core Center and the KAIST Analysis Center for Research Advancement (KARA) for use of confocal microscopes and assistance in performing imaging experiments. **Funding:** This work was supported by grants from the National Research Foundation of Korea (NRF-2022M3E5E8081183 and NRF-2017M3C7A1031322). **Author contributions:** Conceptualization: J.H. and J.-H.H. Data curation: J.H. and J.-H.H. Formal analysis: J.H., B.S., and J.-H.H. Funding acquisition: J.-H.H. Investigation: J.H. and B.S. Methodology: J.H. and J.-H.H. Project administration: J.-H.H. Resources: J.-H.H. Software: J.H. Supervision: J.-H.H. Validation: J.H., B.S., and J.-H.H. Visualization: J.H. and J.-H.H. Writing—original draft: J.H. and J.-H.H. Writing—review and editing: J.H., B.S., and J.-H.H. **Competing interests:** The authors declare that they have no competing interests. **Data and materials availability:** All data needed to evaluate the conclusions in the paper are present in the paper and/or the Supplementary Materials.

Submitted 8 October 2024
Accepted 8 April 2025
Published 9 May 2025
10.1126/sciadv.adt6996